Annals of Biomedical Engineering, Vol. 19, pp. 345–382, 1991
Printed in the USA. All rights reserved.

0090-6964/91 $3.00 + .00
Copyright © 1991 Pergamon Press plc

Wiener Analysis of Nonlinear Feedback in Sensory Systems

Vasilis Z. Marmarelis

Departments of Biomedical and Electrical Engineering
University of Southern California
Los Angeles, CA

(Received 2/4/91; Revised 3/21/91)

Experimental studies of certain sensory systems (e.g., vertebrate retinal cells and auditory fibers) have yielded qualitative evidence of the presence of nonlinear feedback. However, no methods have been available to provide the tools for quantitative analysis of this nonlinear feedback mechanism and subsequent modeling of the overall dynamics of these sensory systems. Recent results offer the analytical means to relate Wiener kernel measurements with corresponding nonlinear feedback models and, thus, the ability to model the overall dynamics of such sensory systems. Furthermore, our analytical results offer an explanation for experimentally observed changes in the waveform of Wiener kernel estimates obtained for different white-noise input mean and/or power levels.

Keywords—*Nonlinear feedback, Wiener analysis, Sensory systems.*

INTRODUCTION

The use of the Wiener approach in modeling studies of nonlinear physiological systems has been expanding in recent years (see, for instance, the edited volumes [11,13]), because it does not require prior knowledge of the internal structure or functional organization of the system and yields models that are true to the data (i.e., they do not reflect subjective biases of the investigator). The practical limitations of this approach have concerned primarily the requirement of white-noise test inputs and the computational burden associated with the estimation of high-order Wiener kernels (9). These limitations have been relaxed by recent findings (for instance, the exact orthogonalization method of Korenberg [7]), even though the computational effort required for the estimation of higher-order (≥ 3) kernels remains beyond the ordinary computing means of most investigators. Furthermore, the representation of higher than second order kernels is a daunting practical problem. Thus, the application of this approach has been practically limited to second-order Wiener models.

Acknowledgments—This work was supported by Grant No. RR-01861 from the National Center for Research Resources of the National Institutes of Health. The author wishes to thank Dr. Møller, Dr. Naka, and Dr. Sakai, whose Wiener kernel measurements in the auditory and visual system have provided the motivation for looking into the properties of nonlinear feedback systems vis-à-vis Wiener analysis. Thanks are also due to my brother Panos, who was the first to suggest (about 18 years ago) the possibility of nonlinear feedback in explaining the experimentally observed changes in horizontal cell kernel waveforms.

Address correspondence to Vasilis Z. Marmarelis, Ph.D., Department of Biomedical Engineering, University of Southern California, Los Angeles, CA 90089-1451.

A more critical problem exists in interpreting the estimated nonlinear Wiener models in a meaningful physiological context. Efforts in this regard have concentrated on the development of relatively simple block-structured models comprised of dynamic linear (L) and static nonlinear (N) components. The most successful block-structured models to date have been cascades of the form L-N, N-L, and L-N-L, although notable attempts have been made in developing models with several parallel channels of such cascades (6,19). Some examples of these efforts are contained in recently edited volumes (11,13), a special issue of the *Annals* (12), and the first book on this subject (9). Although many investigators have made significant contributions in the study of simple cascade models, Korenberg's pioneering paper (5) has been pivotal on this subject. The advantage offered by these block-structured models is compactness, greater interpretability, and the ability to estimate strong nonlinearities (represented by the N components) without resorting to estimation of high-order kernels.

One important class of block-structured models that has not been effectively related to Wiener analysis of experimental data is the one containing nonlinear feedback components. The reason has been the apparent analytical complexity of this class of systems. However, the significance of nonlinear feedback mechanisms for the proper function of physiological systems is unquestionable and has provided the motivation for the present study. Although evidence of nonlinear feedback is found in many physiological systems, our study is concentrated on sensory systems (e.g., visual and auditory), where Wiener kernel measurements have been rather extensive and nonlinear feedback is thought to play an important role.

For instance, it has been observed that several sensory systems undergo a gradual transition from an overdamped to an underdamped dynamic mode (e.g., retinal horizontal cells [10,17]), or the resonance frequency of a band-pass characteristic shifts downward (e.g., auditory nerve fibers [15]) when the power or the mean level of the input signal (stimulus) increases. Simple cascade models of the aforementioned types cannot explain the observed dependence of kernel waveform on stimulus mean and power level, since they can only account for (nonlinear) scaling changes of the kernels. However, a model that employs nonlinear feedback can account for such changes in kernel waveform under various experimental stimulus conditions.

This article addresses the issue of Wiener analysis of a class of nonlinear feedback systems and presents the key analytical expressions that may help interpret Wiener kernel measurements in the aforementioned block-structured modeling context. The guide to this study is provided by the theoretical Volterra-Wiener analysis of a class of nonlinear differential equations that are equivalent representations of a class of nonlinear feedback systems (14). Explicit mathematical expressions have been derived that relate Wiener kernel measurements to the characteristics of the feedback system and the stimulus parameters. Computer simulations have been used to illustrate our theoretical findings and demonstrate analogies in the observed behavior of this class of nonlinear feedback systems with experimental observations from the visual and auditory system that have been previously reported (for instance, [10,15,17]).

VOLTERRA-WIENER ANALYSIS OF A CLASS OF NONLINEAR FEEDBACK SYSTEMS

We consider a nonlinear ordinary differential equation of the form:

$$L(D)y + f(y, Dy, \ldots, D^r y) = M(D)x \tag{1}$$

where D is the differential operator $d(\cdot)/dt$; $x(t)$ and $y(t)$ are the system input and output, respectively; $f(\cdot)$ is a continuous function of its arguments; and $L(D)$, $M(D)$ are polynomials in D (L is of higher degree than r, and M is of lower degree than L). This equation is equivalent to the block-structured system of Fig. 1. If the function $f(\cdot)$ is nonlinear, then the system of Fig. 1 is a nonlinear (negative) feedback system with a linear forward subsystem and a linear subsystem in precascade.

The study of this class of nonlinear feedback systems can be cast in the context of Volterra-Wiener expansions of nonlinear differential equations. To demonstrate this, we consider the case where the function $f(\cdot)$ has only two arguments (y and Dy, the output and its derivative) and is represented by a power series expansion

$$f(y, Dy) = \sum_{i=0}^{\infty} \sum_{\substack{j=0 \\ i+j\geq 2}}^{\infty} c_{i,j} y^i (Dy)^j \tag{2}$$

where the coefficients of the nonlinear terms are of small magnitude; that is, $|c_{i,j}| \leq \epsilon \ll 1$ for all i and j, and ϵ represents the upper bound of the coefficients magnitude. Note that the polynomial $L(D)$ is assumed of degree higher than first (i.e., it involves at least the second derivative of y) and the polynomial $M(D)$ is of lower degree than $L(D)$ by at least two degrees. The nonlinear terms are of degree two and higher since linear terms may be absorbed into $L(D)$, and must be considered as terms of a Taylor (or Weierstrass) expansion of an analytic (or continuous) function of y and its derivative. The constraint on the magnitude of the coefficients $c_{i,j}$ is necessary for simplifying the analytical derivations and corresponds in practice to the requirement of stable behavior of the nonlinear feedback system.

Volterra Series Expansion

For the region of stable solutions of Eq. 1, there exists a Volterra functional expansion (1,2,3,16,20):

$$y(t) = \sum_{n=1}^{\infty} \int_0^{\infty} \cdots \int_0^{\infty} k_n(\tau_1, \ldots, \tau_n) x(t-\tau_1) \cdots x(t-\tau_n)\, d\tau_1 \cdots d\tau_n \tag{3}$$

which represents the system output in terms of a series of multiple convolution integrals of the input. The kernel functions $\{k_n\}$ characterize the dynamics of the nonlinear system and are called the Volterra kernels of the system. They are symmetric

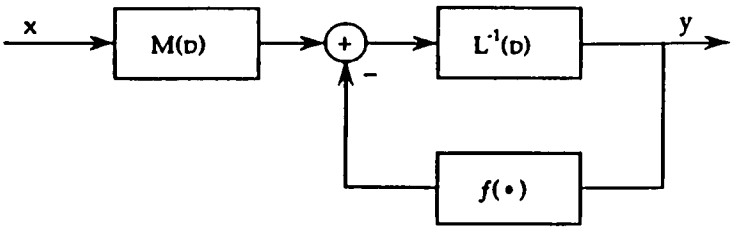

FIGURE 1. Block-structured model of nonlinear feedback system described by the nonlinear differential equation, Eq. 1.

functions of their arguments, that is, attain the same value for all permutations of given $(\tau_1, \ldots, \tau_n)$ values.

A method of generalized harmonic balance can be used to derive analytically the Volterra kernels that correspond to the system described by Eqs. 1 and 2. This method is based on ideas found in (1,3,4,16) and has been detailed in (14). According to this method, the mth order Volterra kernel can be evaluated in the m-dimensional Laplace domain by considering generalized harmonic inputs:

$$x_m(t) = e^{s_1 t} + \cdots + e^{s_m t} \tag{4}$$

where s_i are distinct complex (Laplace) variables. Substitution of the input $x_m(t)$ into Eq. 3 results in the output expression

$$\begin{aligned} y_m(t) &= \sum_{n=1}^{\infty} \sum_{j_1=1}^{m} \cdots \sum_{j_n=1}^{m} e^{(s_{j_1}+\cdots+s_{j_n})t} \\ &\quad \times \int \cdots \int k_n(\tau_1, \ldots, \tau_n) e^{-s_{j_1}\tau_1 - \cdots - s_{j_n}\tau_n} \, d\tau_1 \cdots d\tau_n \\ &= \sum_{n=1}^{\infty} \sum_{j_1=1}^{m} \cdots \sum_{j_n=1}^{m} e^{(s_{j_1}+\cdots+s_{j_n})t} K_n(s_{j_1}, \ldots, s_{j_n}) \end{aligned} \tag{5}$$

and its rth derivative

$$D^r y_m(t) = \sum_{n=1}^{\infty} \sum_{j_1=1}^{m} \cdots \sum_{j_n=1}^{m} (s_{j_1} + \cdots + s_{j_n})^r e^{(s_{j_1}+\cdots+s_{j_n})t} K_n(s_{j_1}, \ldots, s_{j_n}) \tag{6}$$

where K_n is the n-dimensional Laplace transform of the kernel k_n.

Note that the output terms that contain the complex exponential with all *distinct* complex frequencies of the input (i.e., terms of the form $e^{(s_1+\cdots+s_m)t}$) are terms associated with the mth order kernel.

Substitution of the output expression and its derivatives given by Eqs. 5 and 6 into Eq. 1 yields an expression that can be used for the evaluation of the mth order kernel $K_m(s_1, \ldots, s_m)$ on the basis of harmonic balance, that is, by selecting only those terms in the equation that contain the complex exponential $e^{(s_1+\cdots+s_m)t}$ and must balance out. Thus, the harmonic balance approach yields analytical expressions of the Volterra kernels (in ascending order) that depend on the form and parameters of the differential equation.

This procedure has been outlined in detail (14) and yields the following results. The first-order Volterra kernel is evaluated for $m = 1$:

$$K_1(s_1) = \frac{M(s_1)}{L(s_1)} \quad . \tag{7}$$

Note that the nonlinear terms in Eq. 1 do not contribute to K_1 (i.e., the first-order Volterra kernel of the system represents strictly the linear portion of the nonlinear differential equation, as expected).

The second-order kernel is evaluated for $m = 2$:

$$K_2(s_1,s_2) = -\left[c_{2,0} + c_{1,1}\frac{(s_1+s_2)}{2} + c_{0,2}s_1s_2\right]K_1(s_1)K_1(s_2)/L(s_1+s_2) \quad . \tag{8}$$

Continuing on with $m = 3$, we obtain an expression for the third-order kernel when terms of order ϵ^2 or higher are neglected (since we have assumed that $|c_{i,j}| \leq \epsilon \ll 1$):

$$\begin{aligned} K_3(s_1,s_2,s_3) = -\Bigg[c_{3,0} + c_{2,1}\frac{(s_1+s_2+s_3)}{3} + c_{1,2}\frac{(s_1s_2+s_2s_3+s_3s_1)}{3} \\ + c_{0,3}s_1s_2s_3\Bigg]K_1(s_1)K_1(s_2)K_1(s_3)/L(s_1+s_2+s_3) \quad . \end{aligned} \tag{9}$$

Generalizing this analysis and observing that for the mth order harmonic balance of terms containing $e^{(s_1+\cdots+s_m)t}$ the only non-negligible terms (i.e., of order ϵ) will be contributed by the expressions for $y_m(t)$, $D^r y_m(t)$, and $y_m^i(t)[Dy_m(t)]^j$ for $i + j = m$, we have (for $m > 1$):

$$\begin{aligned} K_m(s_1,\ldots,s_m) = -\left\{\sum_{n=0}^{m}\frac{(m-n)!n!}{m!}c_{m-n,n}R_{m,n}(s_1,\ldots,s_m)\right\} \\ \times K_1(s_1)\cdots K_1(s_m)/L(s_1+\cdots+s_m) \end{aligned} \tag{10}$$

where $R_{m,n}(s_1,\ldots,s_m)$ denotes the sum of all distinct products $(s_{j_1}s_{j_2}\cdots s_{j_n})$ that can be formed with combinations of the indices $(j_1,j_2,\ldots,j_n)$ from the set $(1,2,\ldots,m)$. Note that $R_{m,0} = 1$ by definition. Equation 10, in combination with Eq. 7, yields the approximate general expression for the Volterra kernels of this class of nonlinear systems, under the stated assumption of small-magnitude coefficients for the nonlinear terms of Eq. 1.

Wiener Series Expansion

Identification and modeling of a given "black-box" nonlinear system require estimation of the kernels from input-output data. This task is complicated by the fact that the Volterra functional terms are, in general, coupled for a given input, and the problem requires solving a complicated set of simultaneous equations. To solve this estimation problem, Wiener proposed the orthogonalization of the Volterra functional expansion for a Gaussian white noise (GWN) input (21). This leads to decoupling of the functional terms (of the Wiener orthogonal expansion) and allows the estimation of the (Wiener) kernels one at a time.

This approach has been studied extensively in the last 30 years, and the reader is referred to the original Wiener monograph (21) and recent books on the subject (9,11,16,18) for details. A summary, necessary for the developments of this article, follows.

The Wiener orthogonal expansion is:

$$y(t) = \sum_{n=0}^{\infty} G_n[h_n;x(t'),t' \leq t] \tag{11}$$

where the nth order Wiener functional

$$G_n[h_n;x(t'),t' \le t] = \sum_{n=0}^{\infty} \sum_{m=0}^{[n/2]} \frac{(-1)^m n! P^m}{(n-2m)!m!2^m} \times \int_0^{\infty} \cdots \int h_n(\tau_1,\ldots,\tau_{n-2m},\sigma_1,\sigma_1,\ldots,\sigma_m,\sigma_m) \times x(t-\tau_1)\cdots x(t-\tau_{n-2m})\, d\tau_1 \cdots d\tau_{n-2m}\, d\sigma_1 \cdots d\sigma_m \tag{12}$$

contains the nth order Wiener kernel h_n and the power level P of the GWN input.

The most widely used method for the estimation of Wiener kernels has been the cross-correlation technique (8), according to which the nth order Wiener kernel can be estimated from high-order input-output cross-correlations as

$$h_n(\tau_1 \cdots \tau_n) = \frac{1}{n!P^n} E[y_n(t)x(t-\tau_1)\cdots x(t-\tau_n)] \tag{13}$$

where $y_n(t)$ is the nth order output residual:

$$y_n(t) = y(t) - \sum_{m=0}^{n-1} G_m[h_m;x(t',t' \le t)] \ . \tag{14}$$

As indicated by Eqs. 13 and 14, the kernels are estimated successively, in ascending order. In practice the ensemble-average of Eq. 13 is evaluated as a time-average over the experimental input-output record under the assumption of system stationarity. Issues of actual implementation and estimation accuracy in this approach have been addressed extensively (9).

The cross-correlation technique requires fairly long data records to yield kernel estimates of sufficient accuracy. The exact orthogonalization technique proposed recently by Korenberg (6,7) reduces significantly these requirements and leads to estimates of higher accuracy. It also allows certain deviations from whiteness in the experimental input. Likewise, we have recently implemented a method utilizing Laguerre expansions of the kernels and least-squares fitting to obtain improved kernel estimates under the same conditions (i.e., short data records and deviations from whiteness). Thus, these recent techniques offer significantly improved estimation tools for kernels up to second order, relative to the traditional cross-correlation technique.

The Wiener kernels are, in general, different from the Volterra kernels of a given system (for which both expansions exist). The nth order Wiener kernel can be expressed in terms of the Volterra kernels of the same and higher order as (9):

$$h_n(\tau_1,\ldots,\tau_n) = \sum_{m=0}^{\infty} \frac{(n+2m)!P^m}{n!m!2^m} \times \int_0^{\infty} \cdots \int k_{n+2m}(\tau_1,\ldots,\tau_n,\sigma_1,\sigma_1,\ldots,\sigma_m,\sigma_m)\, d\sigma_1 \cdots d\sigma_m \ . \tag{15}$$

The relation between Volterra and Wiener kernels in the frequency domain is

$$H_n(j\omega_1,\ldots,j\omega_n) = \sum_{m=0}^{\infty} \frac{(n+2m)!P^m}{n!m!2^m(2\pi)^m} \int_{-\infty}^{\infty} \cdots \int K_{n+2m} \times (j\omega_1,\ldots,j\omega_n,ju_1,-ju_1,\ldots,ju_m,-ju_m)\,du_1\cdots du_m. \tag{16}$$

For the specific class of systems described by Eq. 1, the Volterra kernels of order higher than first have the approximate form given by Eq. 10. Therefore, combining Eq. 10 with Eq. 15 we can obtain, in first approximation, the general expressions for the high-order Wiener kernels of this class of systems.

The general expression for the first-order Wiener kernel is:

$$H_1(j\omega) = K_1(j\omega) + \sum_{m=1}^{\infty} \frac{(2m+1)!P^m}{m!2^m(2\pi)^m} \times \int_{-\infty}^{\infty} \cdots \int K_{2m+1}(j\omega,ju_1,-ju_1,\ldots,ju_m,-ju_m)du_1\cdots du_m \tag{17}$$

which indicates that $H_1(j\omega)$ is a power series in P and depends on all odd-order Volterra kernels of the system. Note that $H_1(j\omega)$ coincides with $K_1(j\omega)$ (which represents the linear portion of the differential equation) for $P = 0$, as expected. Substituting $K_{2m+1}(\ )$ from the general expression of Eq. 10, we obtain the expression of $H_1(j\omega)$ for the considered class of systems:

$$H_1(j\omega) = K_1(j\omega) - \frac{K_1(j\omega)}{L(j\omega)} \sum_{m=1}^{\infty} \sum_{n=0}^{2m+1} \frac{(2m-n+1)!n!}{m!} \left(\frac{P}{4\pi}\right)^m c_{2m+1-n,n} \times \int_{-\infty}^{\infty} \cdots \int R_{2m+1,n}(j\omega,ju_1,-ju_1,\ldots,ju_m,-ju_m) \times |K_1(u_1)\cdots K_1(u_m)|^2\,du_1\cdots du_m\ . \tag{18}$$

Inspection of the function $R_{2m+1,n}(j\omega,ju_1,-ju_1,\ldots,ju_m,-ju_m)$, as defined following Eq. 10, indicates that its values for n even do not depend on ω, whereas its values for n odd depend linearly on $(j\omega)$. This leads to the following simplified expression:

$$H_1(j\omega) = K_1(j\omega) - \frac{K_1(j\omega)}{L(j\omega)} \sum_{m=1}^{\infty} \frac{(P/2)^m}{m!} \times \sum_{l=0}^{m} [(2m-2l+1)!\,(2l)!\,c_{2m-2l+1,2l} + (j\omega)(2m-2l)!\,(2l+1)!\,c_{2m-2l,2l+1}]\,Q_{m,l} \tag{19}$$

where

$$Q_{m,l} = \frac{1}{(2\pi)^m} \int_{-\infty}^{\infty} \cdots \int R_{m,l}(u_1^2, \ldots, u_m^2) |K_1(u_1) \cdots K_1(u_m)|^2 \, du_1 \cdots du_m \quad . \quad (20)$$

Considering the definition of $R_{m,l}$, we see that the constants $Q_{m,l}$ depend on the Euclidian norms of $|K_1(u)|$ and $|uK_1(u)|$. For these quantities to be finite, the degree of the polynomial $L(D)$ in Eq. 1 must be at least two degrees higher than the polynomial $M(D)$. Thus, Eq. 19 can be written as

$$\begin{aligned} H_1(j\omega) &= K_1(j\omega) - \frac{K_1(j\omega)}{L(j\omega)} [A(P) + j\omega B(P)] \\ &= K_1(j\omega) \left[1 - \frac{A(P) + j\omega B(P)}{L(j\omega)} \right] \end{aligned} \quad (21)$$

where $A(P)$ and $B(P)$ are power series in P with coefficients dependent on $\{Q_{m,l}\}$ and $\{c_{i,j}\}$ for $(i+j)$ odd—that is, i odd and j even for $A(P)$, and i even and j odd for $B(P)$ coefficients. Equation 21 indicates that $H_1(j\omega)$ is affected by the nonlinear terms of Eq. 1 for which $(i+j)$ is odd and depends on the power level P of the GWN input. This explains why first-order Wiener kernel measurements of this class of systems change in waveform as the GWN input power level P changes.

THE CASE OF STATIC NONLINEAR FEEDBACK

A special case of considerable practical interest is when the nonlinearity involves only the output variable, y, and not its derivatives, that is,

$$L(D)y + \epsilon f(y) = M(D)x \quad (22)$$

where $|\epsilon| \ll 1$. If the function $f(\ )$ is analytic or can be approximated to an arbitrary degree of accuracy by a power series (note that the linear term is excluded since it can be absorbed into L),

$$f(y) = \sum_{n=2}^{\infty} \alpha_n y^n \quad (23)$$

then the resulting Volterra kernels are

$$K_1(s) = \frac{M(s)}{L(s)} \quad (24)$$

$$K_n(s_1, \ldots, s_n) = -\epsilon \alpha_n K_1(s_1) \cdots K_1(s_n) / L(s_1 + \cdots + s_n) \quad (25)$$

where terms of order ϵ^2 or higher have been considered negligible.

The first-order Wiener kernel in this case is (cf. Eq. 17)

$$\begin{aligned} H_1(j\omega) &= K_1(j\omega)\left\{1 - \frac{\epsilon}{L(j\omega)} \sum_{m=1}^{\infty} \frac{(2m+1)!}{m!} \left(\frac{P\kappa}{2}\right)^m \alpha_{2m+1}\right\} \\ &= K_1(j\omega)\left[1 - \frac{\epsilon}{L(j\omega)} C_1(P)\right] \end{aligned} \tag{26}$$

where

$$\kappa = \frac{1}{2\pi} \int_{-\infty}^{\infty} |K_1(u)|^2 du \tag{27}$$

and the second-order Wiener kernel is

$$\begin{aligned} H_2(j\omega_1, j\omega_2) &= -\epsilon \frac{K_1(j\omega_1)K_1(j\omega_2)}{L(j\omega_1 + j\omega_2)} \sum_{m=0}^{\infty} \frac{(2m+2)!}{m!2} \left(\frac{P\kappa}{2}\right)^m \alpha_{2m+2} \\ &= -\epsilon \frac{K_1(j\omega_1)K_1(j\omega_2)}{L(j\omega_1 + j\omega_2)} C_2(P) \ . \end{aligned} \tag{28}$$

We observe that, as the input power level varies, the waveform of the first-order Wiener kernel changes but the second-order Wiener kernel remains unchanged in shape and changes only in scale. Note that the functions $C_1(P)$ and $C_2(P)$ are power series (or polynomials) in $(P\kappa)$ and characteristic of the system nonlinearities; furthermore, the Wiener kernels approach their Volterra counterparts as the input power level diminishes (as expected).

These results indicate that, for a system with linear forward and weak nonlinear feedback (i.e., $|\epsilon\alpha_i| \ll 1$), the first-order Wiener kernel in the time domain will be

$$h_1(\tau) = k_1(\tau) - \epsilon C_1(P) \int_0^{\tau} k_1(\tau - \lambda) g(\lambda)\, d\lambda \tag{29}$$

and the second-order Wiener kernel will be

$$h_2(\tau_1, \tau_2) = -\epsilon C_2(P) \int_0^{\min(\tau_1, \tau_2)} k_1(\tau_1 - \lambda) k_1(\tau_2 - \lambda) g(\lambda)\, d\lambda \tag{30}$$

where $g(\lambda)$ is the inverse Fourier transform of $1/L(j\omega)$.

EFFECT OF GWN INPUT MEAN LEVEL

A companion issue to that of changing input power level is the effect of changing mean level of the experimental GWN input. This is a rather common situation in experimental investigations of physiological systems, whereby different mean levels are used for the experimental input (with white-noise perturbations superimposed on them) to explore different ranges of the system function (17). The resulting kernels

for each different mean level of the input will vary, in general, for a nonlinear system. To reconcile these different measurements, we can use a reference mean level μ_0 and refer to its corresponding kernels $\{k_n^0\}$ the kernels $\{k_n^\mu\}$ obtained from different mean levels μ, according to the relation

$$k_n^\mu(\tau_1,\ldots,\tau_n) = \sum_{l=0}^{\infty} \frac{(n+l)!}{n!l!}(\mu-\mu_0)^l \times \int_0^\infty \cdots \int k_{n+l}^0(\tau_1,\ldots,\tau_n,\sigma_1,\ldots,\sigma_l)\,d\sigma_1\cdots d\sigma_l \,. \tag{31}$$

The correspondence with the Wiener kernel measurements is given by the relation

$$h_n^\mu(\tau_1,\ldots,\tau_n) = \sum_{m=0}^{\infty}\sum_{l=0}^{\infty} \frac{(n+2m+l)!}{n!m!l!}\left(\frac{P}{2}\right)^m(\mu-\mu_0)^l \int_0^\infty \cdots \int k_{n+2m+l}^0 \times (\tau_1,\ldots,\tau_n,\lambda_1,\lambda_1,\ldots,\lambda_m,\lambda_m,\sigma_1,\ldots,\sigma_l) \times d\lambda_1\cdots d\lambda_m\,d\sigma_1\cdots d\sigma_l \tag{32}$$

and in the frequency domain

$$H_n^\mu(\omega_1,\ldots,\omega_n) = \sum_{m=0}^{\infty}\sum_{l=0}^{\infty} \frac{(n+2m+l)!}{n!m!l!}\left(\frac{P}{4\pi}\right)^m(\mu-\mu_0)^l \int_{-\infty}^\infty \cdots \int K_{n+2m+l}^0 \times (\omega_1,\ldots,\omega_n,u_1,-u_1,\ldots,u_m,-u_m,0,\ldots,0) \times du_1\cdots du_m \,. \tag{33}$$

The first-order Wiener kernel for the class of systems with static nonlinear feedback, discussed earlier, is given in terms of the reference Volterra kernels (when $\mu_0 = 0$) by the expression

$$h_1^\mu(\tau) = k_1(\tau) - \epsilon\int_0^\tau g(\lambda)k_1(\tau-\lambda)\,d\lambda \times \left\{\sum_{\substack{m=0\\ m+l\geq 1}}^{\infty}\sum_{l=0}^{\infty} \frac{(2m+l+1)!}{m!l!}\left(\frac{P\kappa}{2}\right)^m(\mu\gamma)^l\alpha_{2m+l+1}\right\} \tag{34}$$

where

$$\gamma = \int_0^\infty k_1(\lambda)\,d\lambda \tag{35}$$

and all other parameters and functions are as defined before (k_1 is the zero-mean input first-order Volterra reference kernel). Note that the first-order Wiener kernel for $\mu \neq 0$ is also affected by the even-order terms of the nonlinearity, unlike the case of $\mu = 0$ where it is affected only by the odd-order terms of the nonlinearity.

In the following section, we use computer simulations to demonstrate the effect of changing input power level and/or mean level on the waveform of the first-order Wiener kernel, and draw the analogy with changes observed in the first-order Wiener kernels of some sensory systems when the GWN input power level and/or mean level is varied experimentally.

COMPUTER SIMULATIONS OF SYSTEMS WITH STATIC NONLINEAR FEEDBACK

We demonstrate the theoretical results obtained in the previous sections by simulating systems with static nonlinear feedback and observing the effects of various nonlinearities, input power levels, and input mean levels on the estimated Wiener kernels.

Cubic Feedback Systems

First, we consider a system with a low-pass forward linear subsystem (L) and a cubic negative feedback ($f = \epsilon y^3$) as shown in Fig. 1 (for $M \equiv 1$). For $|\epsilon| \ll 1$, the first-order Wiener kernel is (cf. Eq. 29 and note that $g \equiv k_1$ in this case)

$$h_1(\tau) = k_1(\tau) - 3\epsilon P\kappa \int_0^\tau k_1(\lambda)k_1(\tau - \lambda)\, d\lambda \tag{36}$$

where $k_1(\tau)$ is the impulse response function of the low-pass linear forward subsystem (as well as the first-order Volterra kernel of the overall system) shown in Fig. 2. For a zero-mean GWN input with power levels of $P = 1, 2, 4$ and cubic feedback coefficient $\epsilon = 0.01$, we compute the first-order Wiener kernel estimates using 1024 input/output data points and the aforementioned Laguerre expansion technique. The resulting estimates are shown along with the estimate for $\epsilon = 0$ (i.e., no cubic feedback) in Fig. 3. We observe a gradual decrease of damping (i.e., emergence of an "undershoot") in the kernel estimates, consistent with Eq. 36. We can also observe a gradual increase of their bandwidth as the GWN input power level (P) increases, which is demonstrated in Fig. 4, where the FFT magnitude functions of these kernel estimates are shown up to normalized frequency 0.1 Hz (Nyquist frequency is 0.5 Hz). We observe the gradual transition from an overdamped to an underdamped mode and a companion decrease of zero-frequency gain as P increases, similar to what has been observed in certain low-pass sensory systems such as retinal horizontal cells. Note that this system becomes unstable when P increases beyond a certain value.

Next we explore the effect of varying the (GWN) input mean level while keeping ϵ and P constant. We simulate the previous system for $\epsilon = 0.001$ and $P = 1$ using input mean levels $\mu = 0, 1, 2$, and 3, successively. The response amplitude histograms are shown in Fig. 5, and the cubic nonlinearity used in negative feedback is shown in Fig. 6. The obtained first-order Wiener kernel estimates are shown in Fig. 7. We observe that the changes in the waveform of the kernels as the input mean level increases are qualitatively similar to the ones induced by increasing input power level—that is, increasing bandwidth and decreasing damping. According to the general expression of Eq. 34, we have for this system

$$h_1^\mu(\tau) = k_1(\tau) - 3\epsilon[P\kappa + (\mu\gamma)^2] \int_0^\tau k_1(\lambda)k_1(\tau - \lambda)\, d\lambda\ . \tag{37}$$

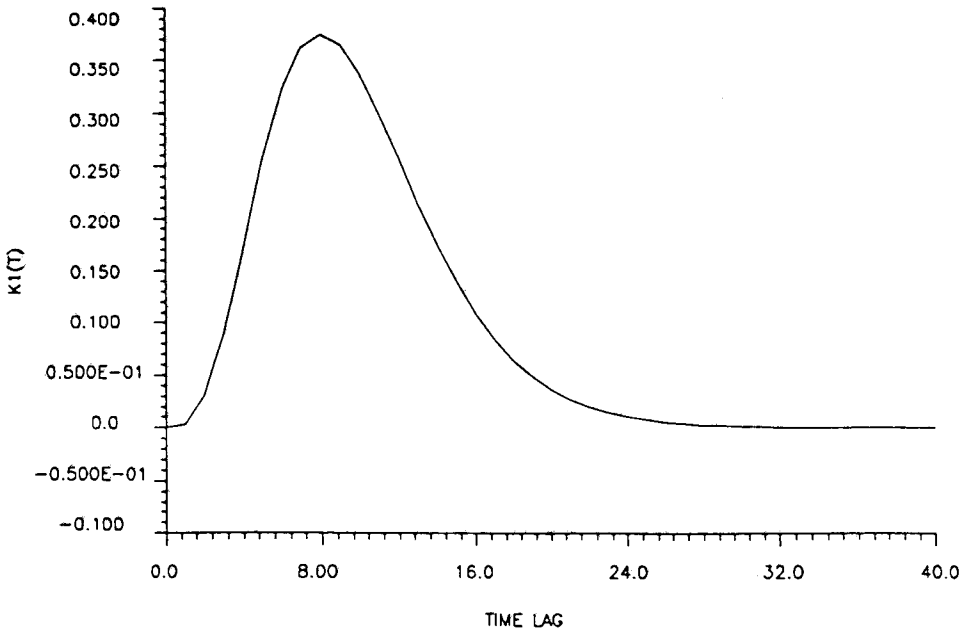

FIGURE 2. Impulse response function of overdamped linear forward subsystem (L-1) used in the first simulation example.

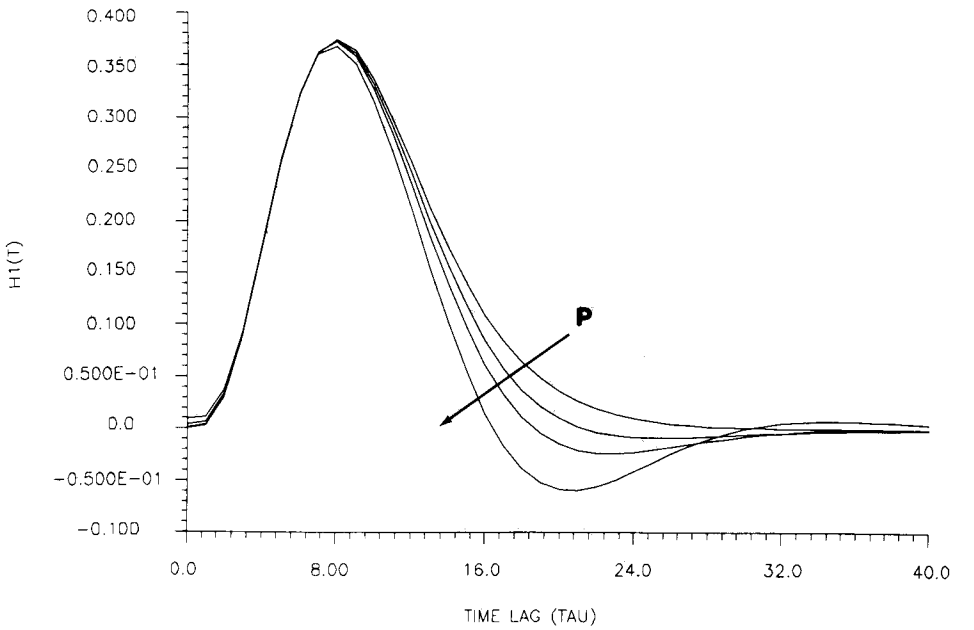

FIGURE 3. First-order Wiener kernel estimates of the system with negative cubic feedback nonlinearity ($\epsilon = 0.001$) and the forward subsystem shown in Fig. 2, for $P = 1$, 2, and 4 along with the first-order Volterra kernel of the system ($P \rightarrow 0$). Observe the changes in kernel waveform as P increases.

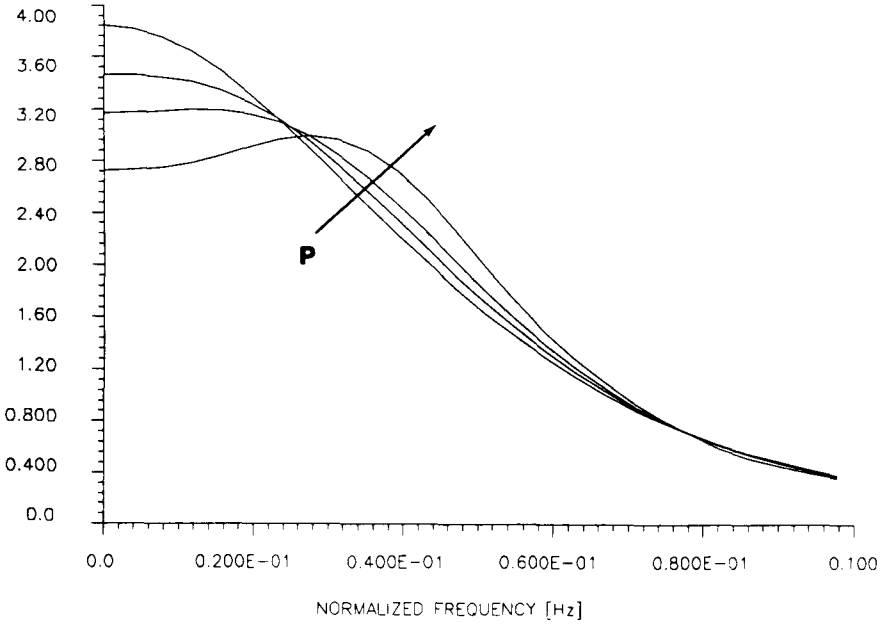

FIGURE 4. FFT magnitudes of the first-order kernels shown in Fig. 3, plotted up to normalized frequency of 0.1 Hz. Observe the increase of system bandwidth as *P* increases.

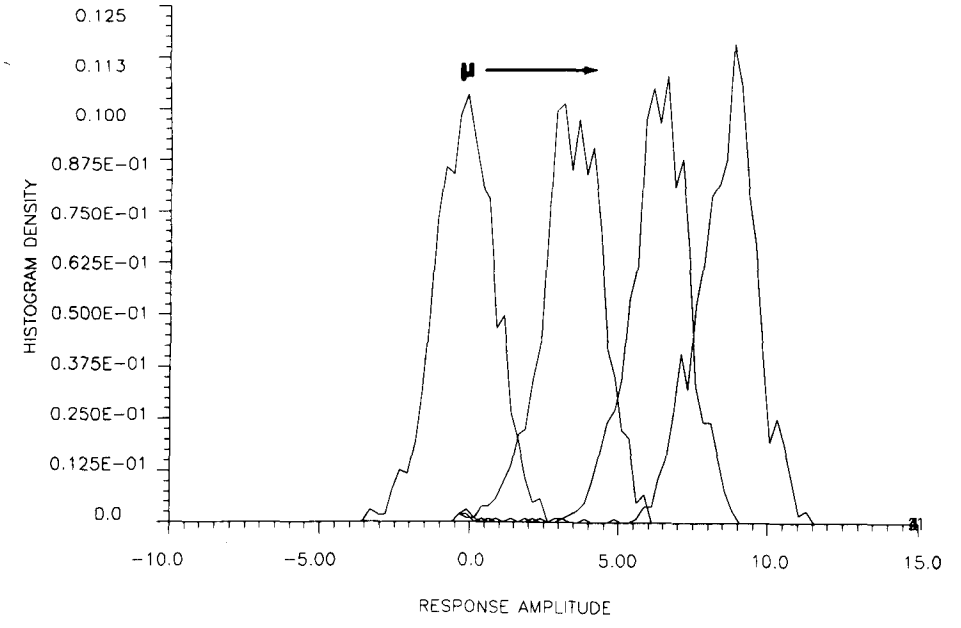

FIGURE 5. Amplitude histograms of negative cubic feedback system responses for GWN inputs ($P = 1$) with mean levels $\mu = 0, 1, 2,$ and 3. Observe that the variance of these histograms does not change significantly, although their mean follows a sublinear relation versus μ.

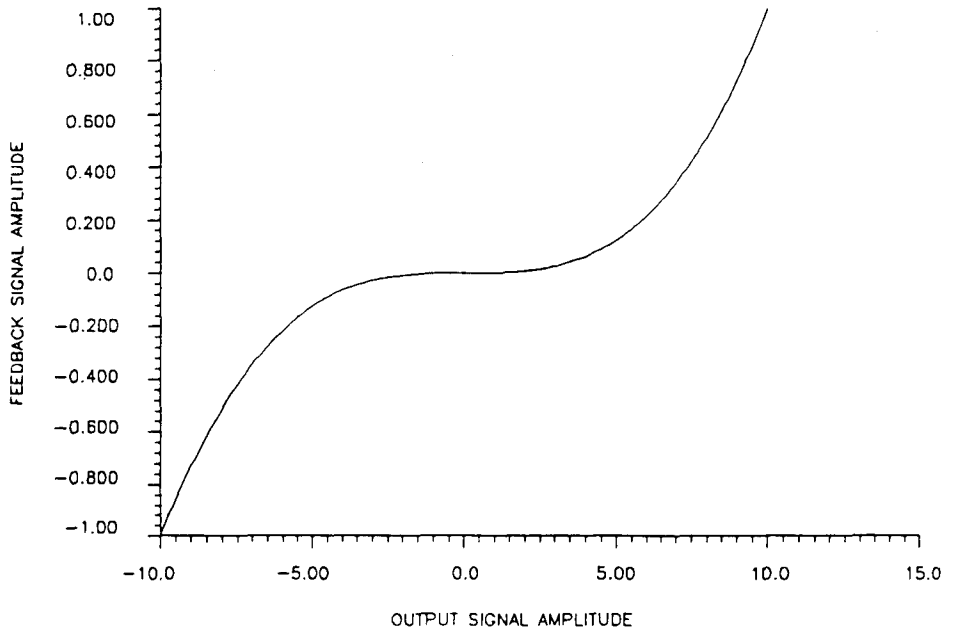

FIGURE 6. Form of the cubic nonlinearity used in negative feedback ($\epsilon = 0.001$).

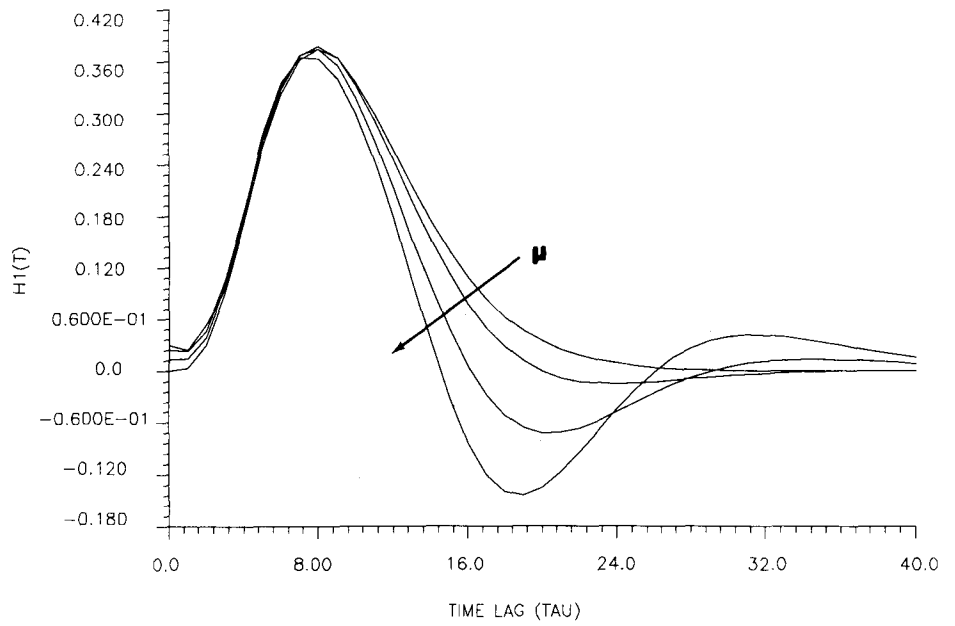

FIGURE 7. First-order Wiener kernel estimates of system with negative cubic feedback nonlinearity and the forward subsystem shown in Fig. 2, for $\mu = 0$, 1, 2, and 3 ($P = 1$, $\epsilon = 0.001$ in all cases). The changes in kernel waveform follow the same pattern as in Fig. 3.

We see that the effect of increasing P is similar to the effect of increasing μ^2 (which also implies that the effect is the same for positive or negative μ) and the differential effect is proportional to κ and γ^2, respectively. The latter observation implies that the differential effect of changing P or μ^2 by the same amount is greater for mean level changes in the case of a low-pass forward subsystem; however, for underdamped or band-pass forward subsystems this differential effect may be reversed.

Another point of practical interest that must be made in connection with this example is the difference between the first-order kernel (Volterra or Wiener) and the system response to an impulse. This point is often the source of confusion due to biases ingrained by linear system analysis. For a third-order system, such as in this example for small ϵ, the response to an impulse input $x(t) = A\delta(t)$ is

$$\begin{aligned} r(t) &= Ak_1(t) + A^3k_3(t,t,t) \\ &= Ak_1(t) - \epsilon A^3 \int_0^t k_1(\lambda)k_1^3(t-\lambda)\,d\lambda \ . \end{aligned} \tag{38}$$

This is clearly different from the first-order Volterra kernel $k_1(t)$ and its Wiener counterpart given by Eq. 36.

Likewise, the response to a step input $x(t) = Au(t)$ is

$$s(t) = A\int_0^t k_1(\tau)\,d\tau - \epsilon A^3 \int_0^t k_1(\tau)\left\{\int_0^t k_1(\lambda-\tau)\,d\lambda\right\}^3 d\tau \ . \tag{39}$$

The changes in pulse response waveforms as the pulse amplitude increases are demonstrated in Fig. 8, where the responses of this system are shown for pulse amplitudes of 1, 2, and 4. The observed changes are qualitatively consistent with the previous discussion (i.e., the responses are less damped for stronger pulse inputs). However, we cannot obtain the first-order Wiener kernel or the response to an impulse by differentiating them in time, as in the linear case. Observe also the sharp difference between on-set and off-set response, characteristic of nonlinear system and so often seen in physiological systems. The steady-state value of the step response for various values of A is given by

$$L(0)y + \epsilon y^3 = A \tag{40}$$

(in the region of stability of this system) where $L(0) = 1/K_1(0)$ for this system. The steady-state values of the pulse response as a function of pulse amplitude are shown in Fig. 9. Note that these values are different, in general, from the mean response value when the GWN input has nonzero mean.

In the next series of simulations, we consider an underdamped linear forward subsystem (its impulse response function shown in Fig. 10) with negative cubic feedback of $\epsilon = 0.008$. The resulting first-order Wiener kernel estimates for increasing GWN input power level (viz., $P = 1$, 2, and 4) are shown in Fig. 11 along with the first-order Volterra kernel of the system (which is the same as the impulse response function of the linear forward subsystem, shown in Fig. 10). We observe a gradual deepening of the undershoot portion of the kernel accompanied by a gradual shortening of its

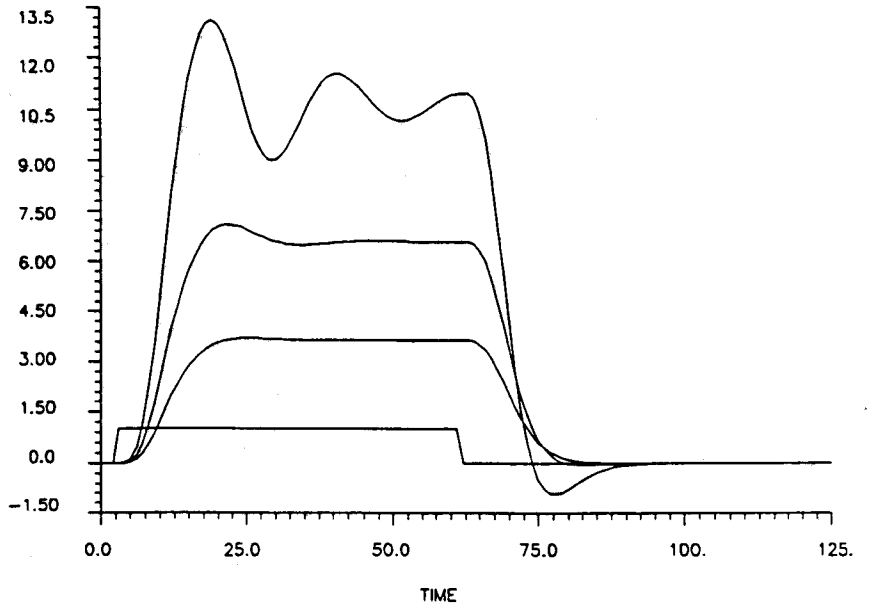

FIGURE 8. Responses of negative cubic feedback system ($\epsilon = 0.001$) to pulse inputs of different amplitudes (1, 2, and 4). Observe the gradual decrease of damping and latency of the on-set response as the pulse amplitude increases, as well as the difference between on-set and off-set responses.

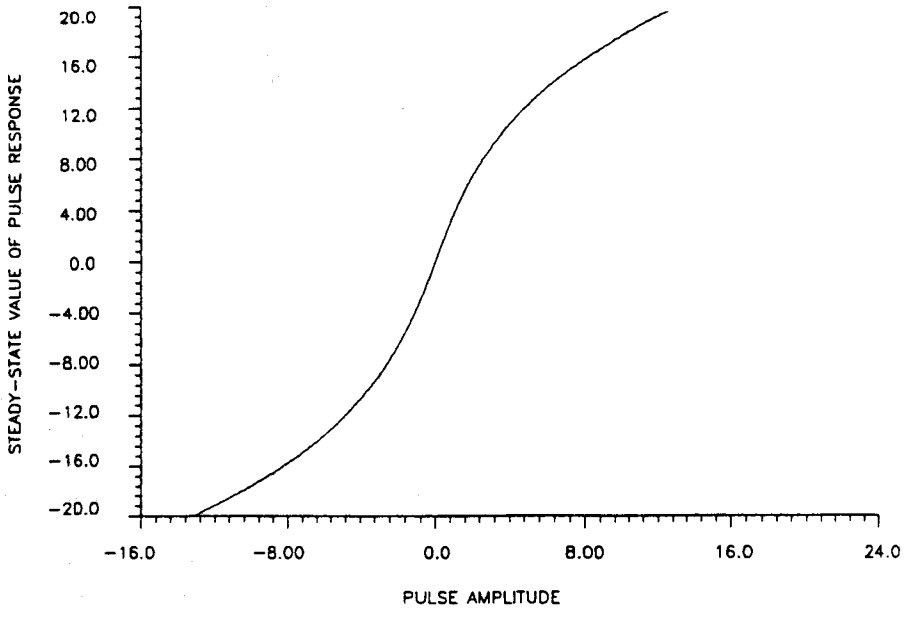

FIGURE 9. The steady-state values of the pulse responses as a function of input pulse amplitude for the negative cubic feedback system ($\epsilon = 0.001$).

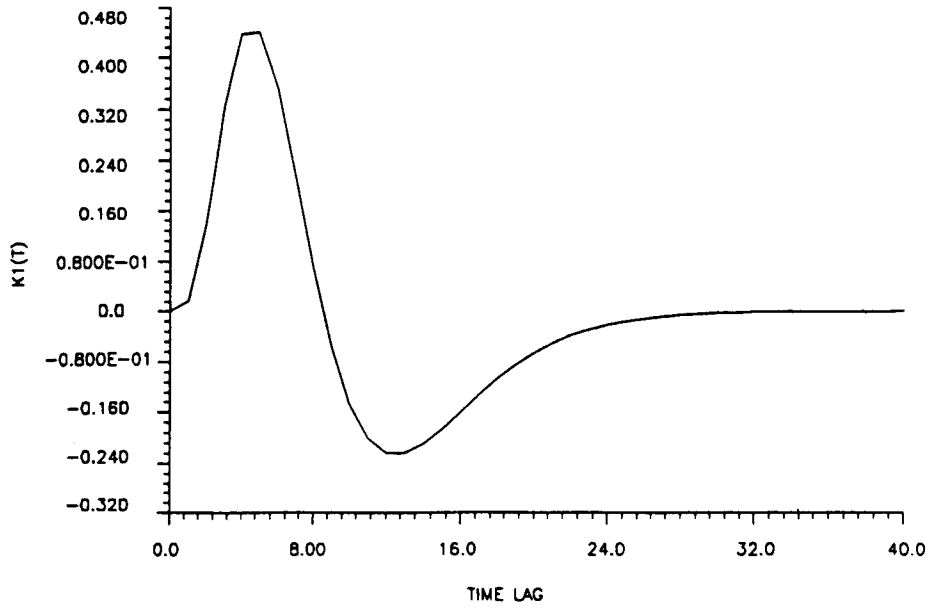

FIGURE 10. Impulse response function of the underdamped linear forward subsystem used in the second simulation example.

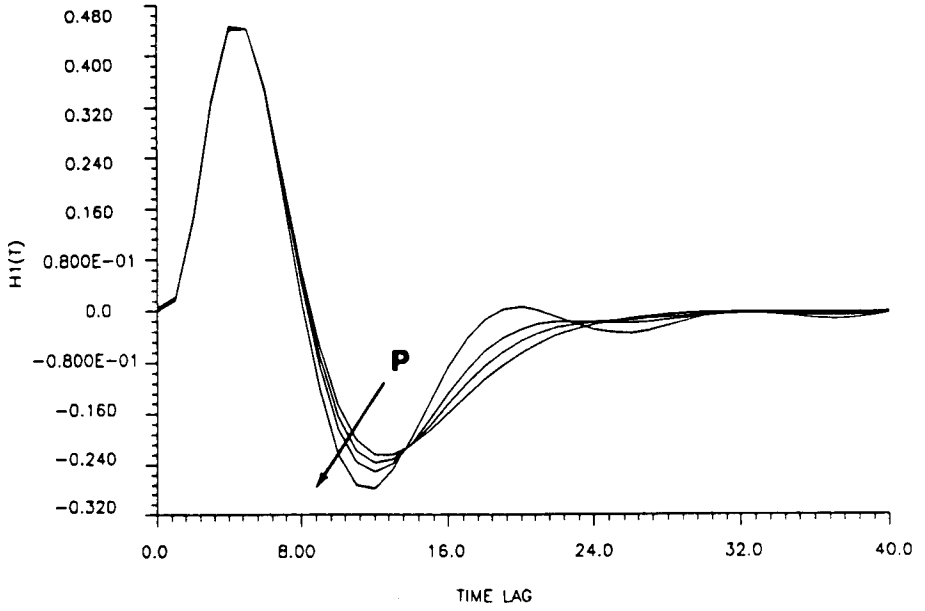

FIGURE 11. First-order Wiener kernels of negative cubic feedback system ($\epsilon = 0.008$) with the underdamped linear forward of Fig. 10, for $P = 0.1$, 1, 2, and 4. Observe the increasing undershoot as P increases.

duration as P increases (i.e., we see a gradual broadening of the system bandwidth and upward shift of the resonance frequency as P increases). This is demonstrated in Fig. 12, where the FFT magnitudes of the kernels of Fig. 11 are shown. The changes in the waveform of these kernels with increasing P are consistent with our theoretical analysis.

Next we compute the first-order Wiener kernels for $\epsilon = 0.008$, $P = 1$, and increasing GWN input mean level. The resulting kernels for $\mu = 0$, 1, 2, and 4 are shown in Fig. 13, and they demonstrate insignificant effect of the nonzero mean levels due to the fact that γ (i.e., the integral of k_1) is extremely small in this case, as predicted by Eq. 37. Finally, the system response to pulses of increasing amplitude ($A = 1$, 2, and 4) are shown in Fig. 14, demonstrating increasing resonance frequency and decreasing damping in the pulse response as A increases. Note also that the steady-state values of the pulse responses are extremely small, and the on-set/off-set response waveforms are similar (with reversed polarity), due to the very small value of $\gamma = K_1(0) = 1/L(0)$ (cf. Eq. 40).

Sigmoid Feedback Systems

The next round of simulations deals with a sigmoid feedback nonlinearity which, unlike the cubic one, is bounded for any response signal amplitude. The following normalized arctangent function, shown in Fig. 15 for $\epsilon = 1$ and $\alpha = 0.25$, was used in the simulations:

$$f(y) = \epsilon \frac{2}{\pi} \arctan(\alpha y) \quad . \tag{41}$$

For the low-pass forward subsystem shown in Fig. 2, the resulting first-order Wiener kernels for $P = 1$ and $\epsilon = 0$, 0.125, 0.25, and 0.5 are shown in Fig. 16 ($\alpha = 0.25$). The qualitative changes in waveform are similar to the cubic feedback case, for increasing feedback strength. However, for fixed sigmoid feedback strength (ϵ) the kernels resulting from increasing GWN input power level P follow the *reverse* transition in waveform. This is demonstrated in Fig. 17, where the kernels obtained for $P = 1$, 4, 16, and 64 are shown ($\epsilon = 0.25$ for all cases). The changes in kernel waveform follow the previously presented analysis, bearing in mind that the first-order Volterra kernel of this system is not the same as the impulse response function of the forward subsystem, but it is the impulse response function of the overall linear feedback system when the linear term of the sigmoid nonlinearity (i.e., its slope at zero) is incorporated in the (negative) feedback loop. Thus, the kernel waveform changes gradually from the impulse response function of the linear feedback system to that of the linear forward subsystem as P increases from very small to very large values. The kernel waveform changes gradually from underdamped to overdamped as P increases (i.e., the gain of the equivalent linearized feedback decreases). This is demonstrated by the kernel FFT magnitudes shown in Fig. 18 for the kernels in Fig. 17.

Because of the bounded nature of the (negative) sigmoid nonlinearity, large values of ϵ and/or P do not lead to system instabilities as in the case of cubic feedback. Increasing values of ϵ result in decreasing damping, eventually leading to oscillatory behavior. This is demonstrated in Fig. 19, where the kernels for $\epsilon = 0.5$, 1, 2, and 4 are shown ($P = 1$). The oscillatory behavior of the system, for very large values of

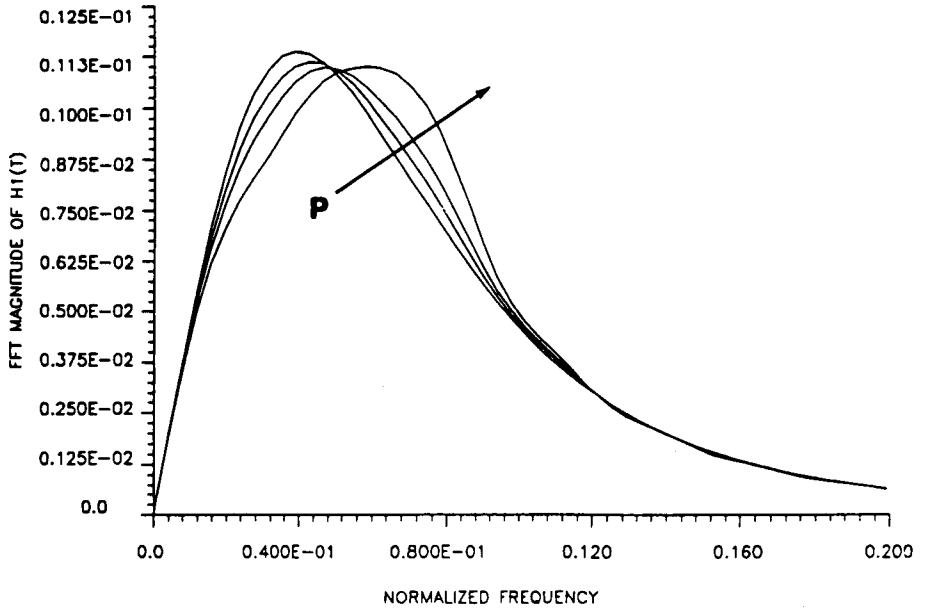

FIGURE 12. FFT magnitudes of the first-order Wiener kernels shown in Fig. 11. Observe the gradual increase of bandwidth and upward shift of resonant frequency as P increases.

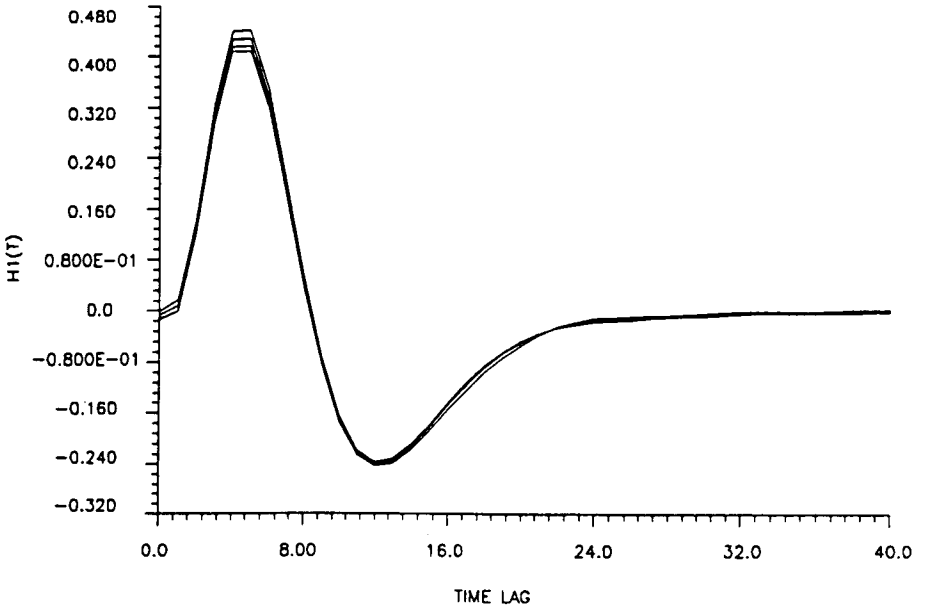

FIGURE 13. First-order Wiener kernels of negative cubic feedback system ($\epsilon = 0.008$) with underdamped forward for different GWN input mean levels $\mu = 0$, 1, 2, and 4 ($P = 1$). Observe the negligible change in kernel waveform as predicted by the analytical derivations.

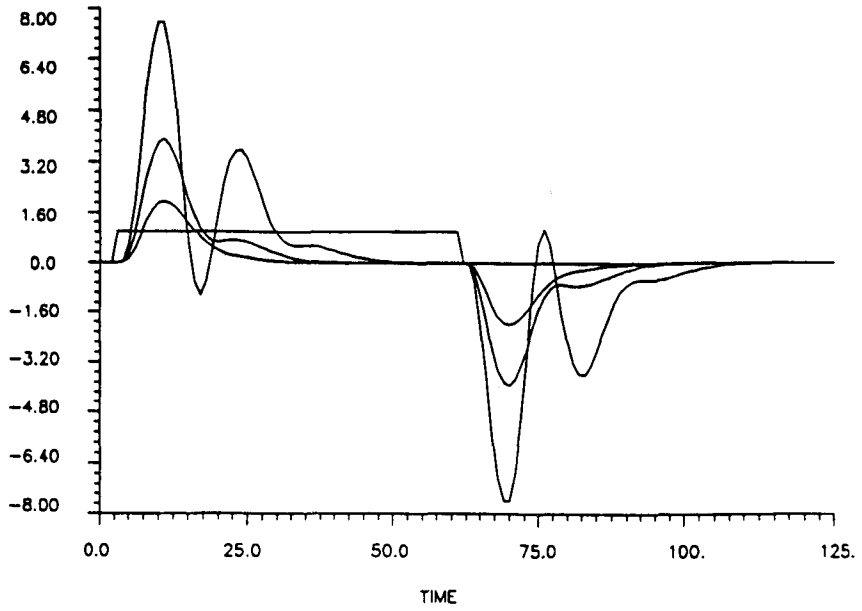

FIGURE 14. Response of negative cubic feedback system ($\epsilon = 0.008$) with underdamped forward to pulse inputs of different amplitudes $A = 1$, 2, and 4. Observe the increasingly underdamped response as A increases, and the negligible steady-state response.

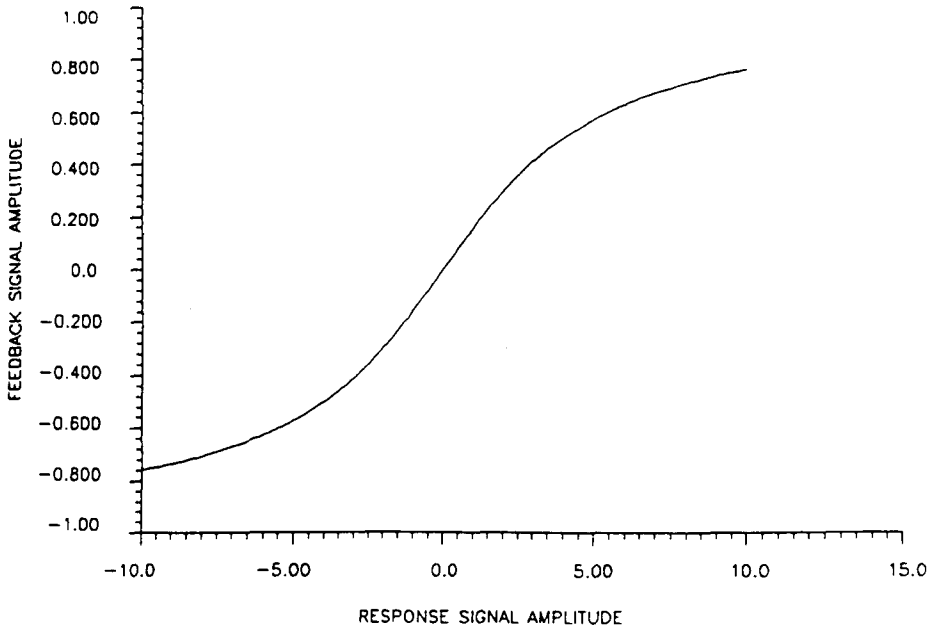

FIGURE 15. Sigmoid feedback nonlinearity $f(y) = (2/\pi)\arctan(y/4)$.

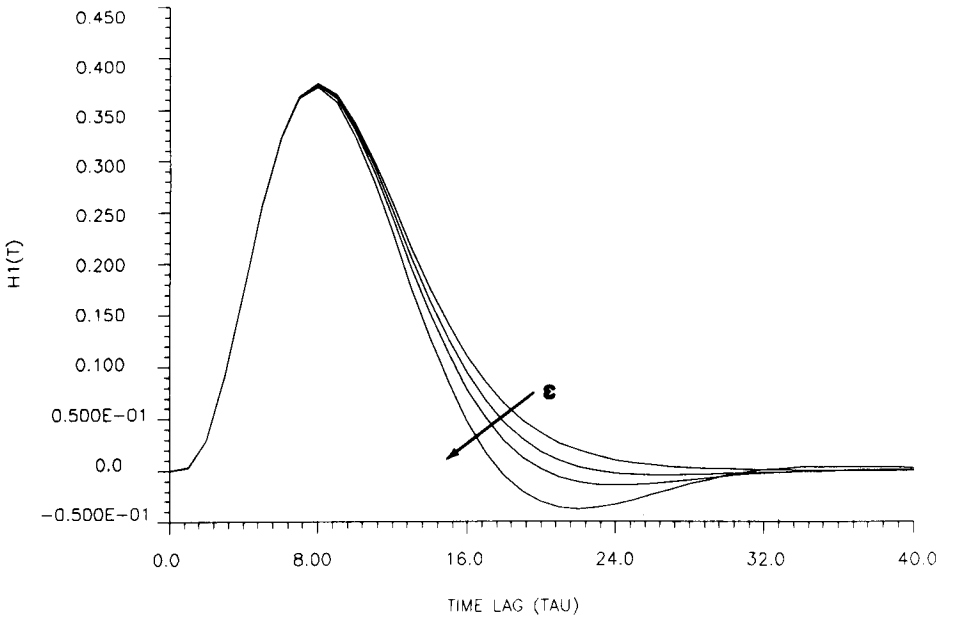

FIGURE 16. First-order Wiener kernel estimates of negative sigmoid feedback system with the forward subsystem shown in Fig. 2, for $\epsilon = 0$, 0.125, 0.25, and 0.5 ($P = 1$, $\alpha = 0.25$ in all cases). Observe the similarity in changes of kernel waveform with the ones shown in Fig. 3.

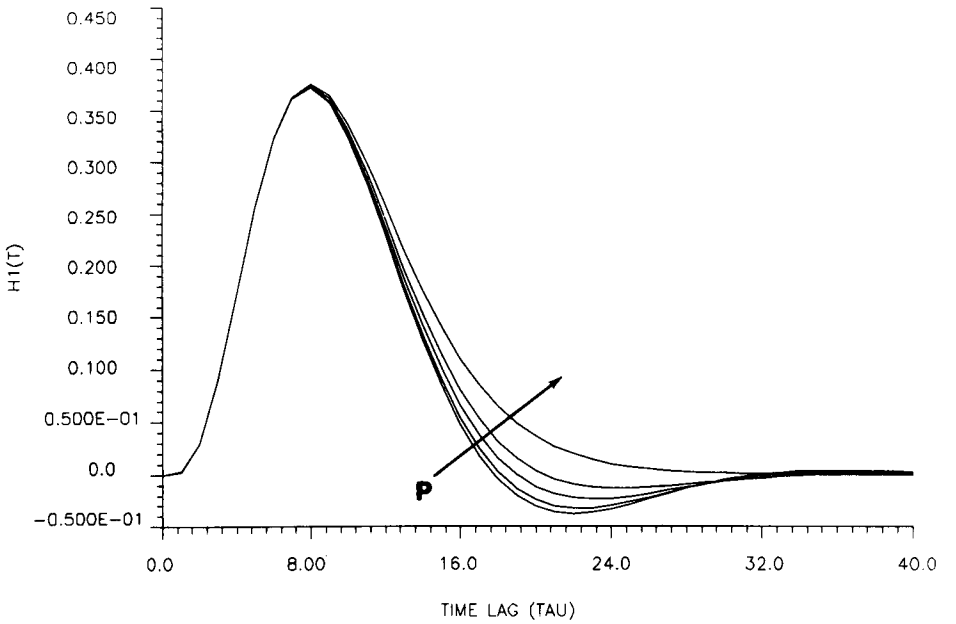

FIGURE 17. First-order Wiener kernel estimates of negative sigmoid feedback system with the forward subsystem shown in Fig. 2, for $P = 1$, 4, 16, and 64 ($\epsilon = 0.25$, $\alpha = 0.25$ in all cases). Observe reverse pattern of kernel waveform changes from the one in Fig. 16.

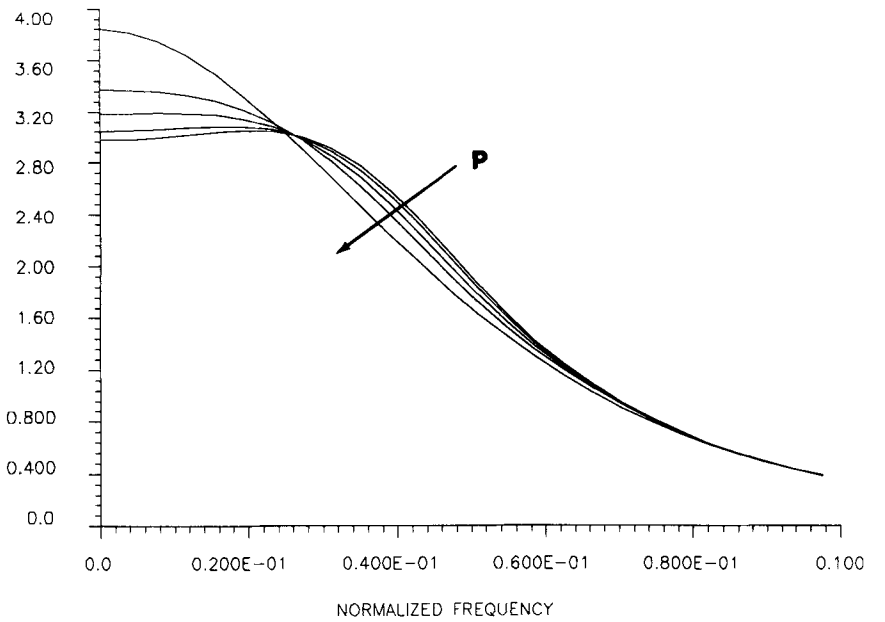

FIGURE 18. FFT magnitudes of kernels shown in Fig. 17, plotted up to normalized frequency of 0.1 Hz. Observe transition to narrower bandwidth as *P* increases.

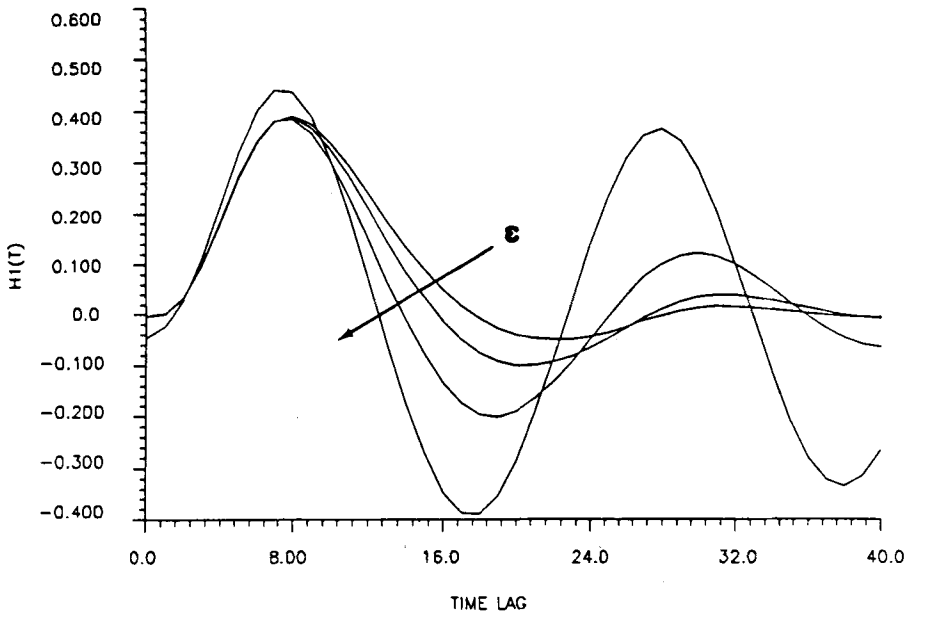

FIGURE 19. First-order Wiener kernels of negative sigmoid feedback system with overdamped forward, for $\epsilon = 0.5$, 1, 2, and 4. Observe transition to oscillatory behavior as ϵ increases.

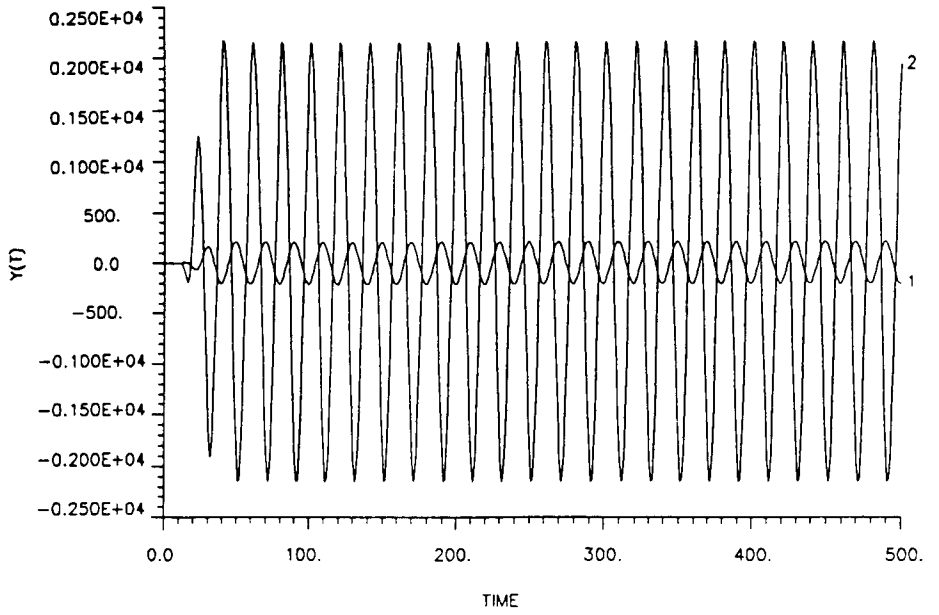

FIGURE 20. Oscillatory response of negative sigmoid feedback system for GWN input ($P = 1$) and $\epsilon = 100$ and 1000.

ϵ, is more dramatically demonstrated in Fig. 20, where the actual system responses $y(t)$ for $\epsilon = 100$ and 1000 are shown ($P = 1$). The system goes into perfect oscillation regardless of the GWN input, due to the overwhelming action of the negative sigmoid feedback that is both bounded and symmetric about the origin. The amplitude of this oscillation is proportional to ϵ, but it is independent of the input power level. In fact, the oscillatory response remains the same in amplitude and frequency for any input signal (regardless of its amplitude and waveform) as long as the value of ϵ is much larger than the maximum value of the input. The initial transient and the phase of the oscillation, however, may vary according to the input power and waveform. The frequency of the oscillation depends on the linear forward subsystem. For instance, a low-pass subsystem with shorter memory (i.e., shorter time support) leads to higher frequency of oscillation, and so does an underdamped system with the same memory extent.

The case of oscillatory behavior due to large sigmoid negative feedback is not covered by the Volterra-Wiener analysis presented in the previous section. It is, however, of great interest in physiology because of the numerous and functionally important physiological oscillators. It is a subject worthy of further exploration, albeit outside the scope of this article.

The effect of varying the slope of the sigmoid nonlinearity is demonstrated in Fig. 21, where the first-order kernels for $\epsilon = 1$, $P = 1$, and slopes $\alpha = 0.125$, 0.25, 0.5, and 1 are shown. We observe gradually decreasing damping with increasing slope. This transition reaches asymptotically a limit in both directions of changing α values,

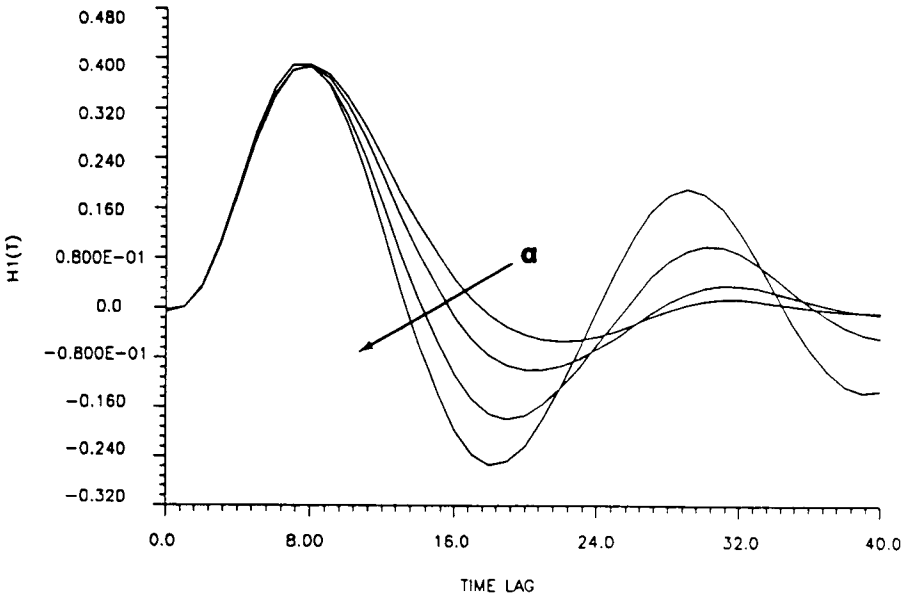

FIGURE 21. First-order Wiener kernels of negative sigmoid feedback system ($\epsilon = 1$, $P = 1$) for increasing slope of sigmoid curve: $\alpha = 0.125$, 0.25, 0.5, and 1. Observe that kernel waveform changes are qualitatively similar with increasing ϵ (see Fig. 19).

as expected. For $\alpha \to \infty$, the sigmoid nonlinearity becomes the signum function and leads to perfect oscillations; and for $\alpha \to 0$ the gain of the feedback loop diminishes leading to a kernel identical to the impulse response function of the forward linear subsystem.

The effect of nonzero input mean level is demonstrated in Fig. 22, where the kernels for $\mu = 0$, 1, 2, and 4 are shown ($\epsilon = 1$, $P = 1$, $\alpha = 0.25$). The kernels become more damped as the GWN input mean level increases, following the transition pattern of increasing input power level (i.e., decreasing gain of the equivalent linearized feedback).

In the case of the underdamped forward subsystem shown in Fig. 10 and sigmoid (negative) feedback, the results are qualitatively similar to the previous case. The changes in the kernel waveform undergo a gradual transition from the linearized feedback system to the forward linear subsystem as the GWN input power level increases from very small to very large values. The two limit kernel waveforms (for $P \to 0$ and $P \to \infty$) are shown in Fig. 23 for $\epsilon = 1$, $\alpha = 0.25$. The effect of the sigmoid feedback is less dramatic in this case, since the kernel retains its underdamped mode for all values of P. There is, however, a downward shift of resonance frequency and increase of damping when P increases, as indicated by the FFT magnitudes of the "limit" kernel waveforms (of Fig. 23) shown in Fig. 24.

Positive Nonlinear Feedback

The reverse transition in kernel waveform is observed when the polarity of small nonlinear feedback is changed, according to Eq. 37. Positive decompressive (e.g., cu-

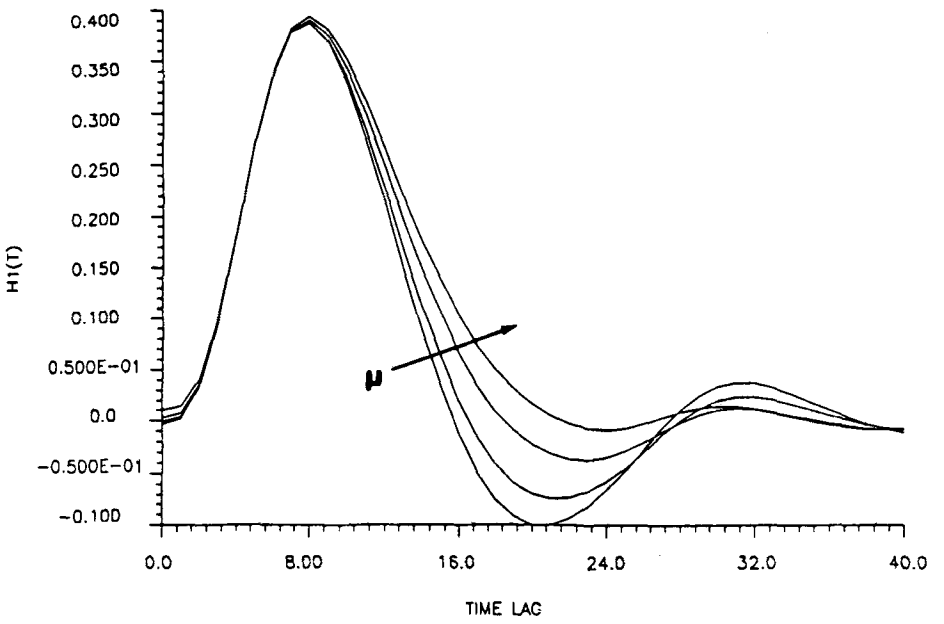

FIGURE 22. First-order Wiener kernels of negative sigmoid feedback system ($\epsilon = 1$, $P = 1$, $\alpha = 0.25$) for different GWN input mean levels $\mu = 0$, 1, 2, and 4. Observe that kernel waveform changes are similar with increasing P (see Fig. 17).

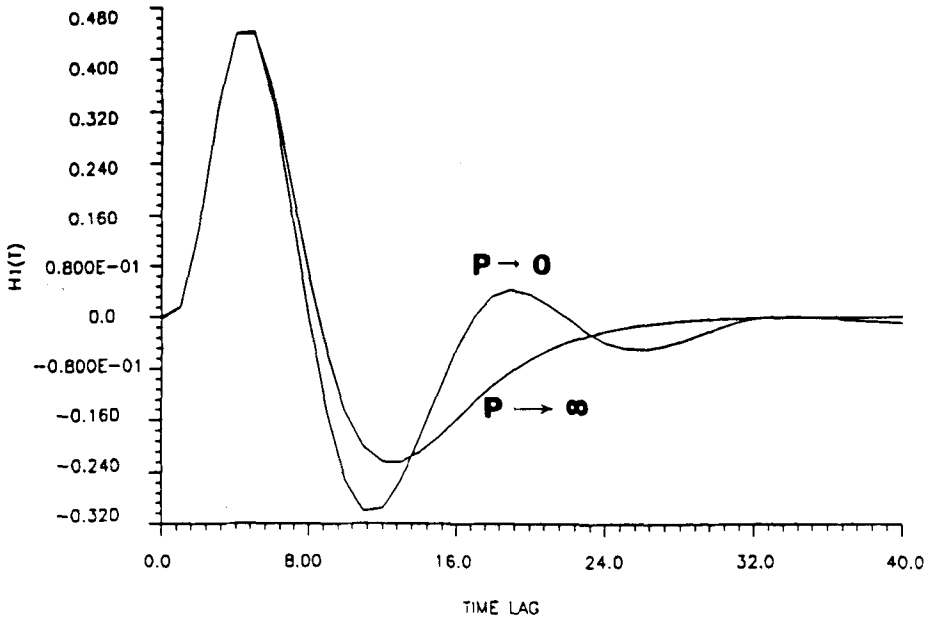

FIGURE 23. The two limit Wiener kernel waveforms of negative sigmoid feedback system ($\epsilon = 1$, $\alpha = 0.25$) with underdamped forward, obtained for $P \to 0$ and $P \to \infty$.

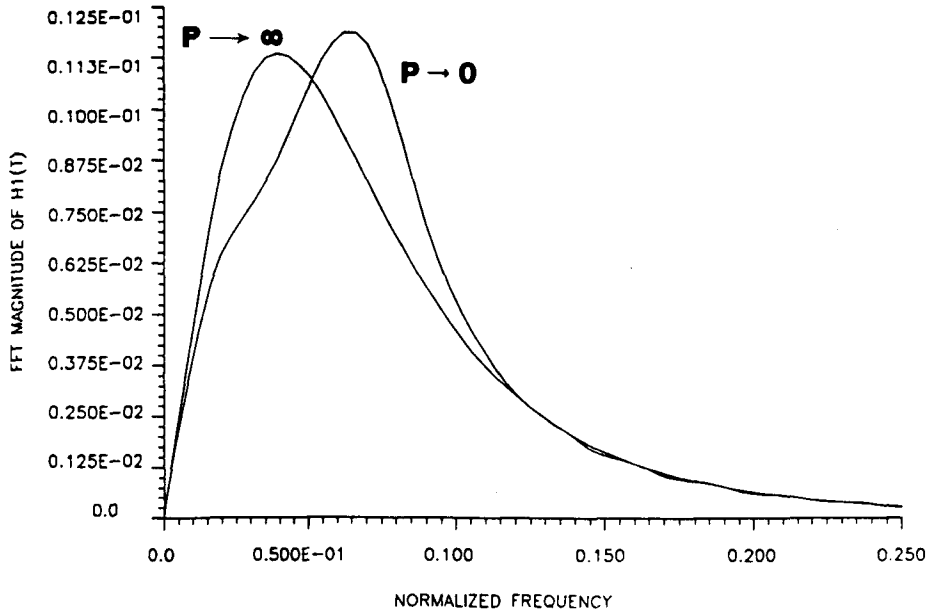

FIGURE 24. FFT magnitudes of the two limit kernel waveforms shown in Fig. 23. Observe the lower frequency for $P \to \infty$.

bic) feedback leads to a decrease in resonance frequency and higher gain values in the resonant region. The reverse transition in kernel waveform occurs (i.e., upward shift of resonance frequency and decrease of damping with increasing P values) when compressive (e.g., sigmoid) feedback becomes positive.

The great advantage of sigmoid versus cubic feedback is that stability of the system behavior is retained over a broader range of the input power level. For this reason, sigmoid feedback is an appealing candidate for models of physiological feedback systems. For those systems that exhibit transitions to broader bandwidth and decreased damping as P increases, candidate models may include either negative decompressive (e.g., cubic) feedback or positive compressive (e.g., sigmoid) feedback. For those systems that exhibit the reverse transition patterns (i.e., to narrower bandwidth and increased damping) as P increases, candidate models may include either positive decompressive or negative compressive feedback.

Second-Order Kernels of Nonlinear Feedback Systems

Our examples so far have employed nonlinear feedback with odd symmetry (cubic and sigmoid), and our attention has focused on first-order Wiener kernels of the resulting systems. These systems do not have even-order kernels. However, if the feedback nonlinearity is not odd-symmetric, then even-order kernels exist. An example of this is given for quadratic feedback when the underdamped linear forward subsystem is the one shown in Fig. 10. Simulations were made for negative quadratic feedback of the form ϵy^2, for $\epsilon = 0.08$ ($P = 1$), and the resulting second-order Wiener kernel estimate is shown in Fig. 25. It has the approximate form and size predicted

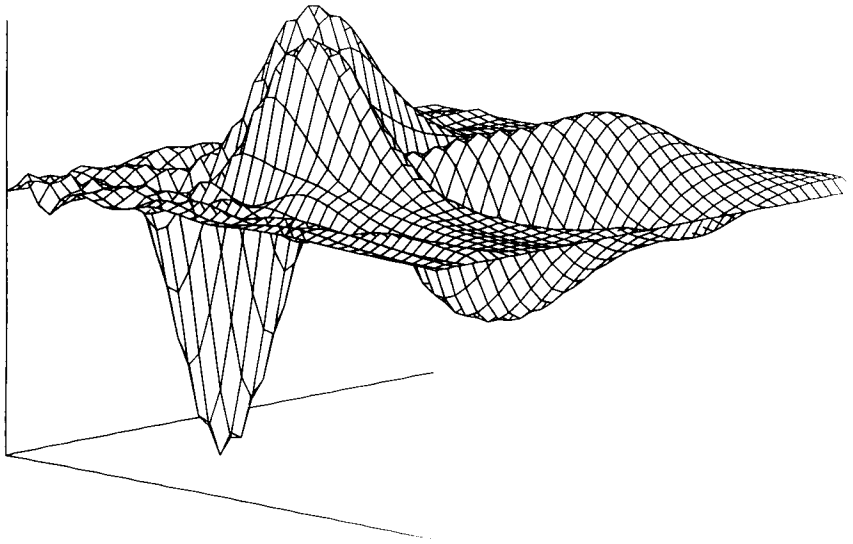

FIGURE 25. Second-order Wiener kernel estimate for negative quadratic feedback system with linear underdamped forward ($\epsilon = 0.08$, $P = 1$).

by our analytical derivations (cf. Eq. 30) as indicated by the exact second-order kernel shown in Fig. 26. The first-order Wiener kernels are not affected by the quadratic feedback for small values of ϵ.

It is important to note that, although the cubic or sigmoid feedback systems have no even-order Volterra kernels, Wiener analysis of these systems with nonzero GWN input mean yields even-order Wiener kernels dependent on the nonzero input mean (cf. Eq. 32). This point was discussed earlier, and general expressions were derived that relate the Wiener kernels for GWN input mean μ to reference Volterra kernels corresponding to a reference input mean μ_0 (see Eqs. 32 and 33). Consider, for instance, a negative cubic feedback system where only K_1 and K_3 are assumed to be significant for small values of ϵ. Then the theoretically derived Eq. 33 yields (for $n = 2$)

$$\begin{aligned} H_2^{\mu}(\omega_1,\omega_2) &= 3\mu K_3(\omega_1,\omega_2,0) \\ &= -3\epsilon\mu\gamma K_1(\omega_1)K_1(\omega_2)K_1(\omega_1+\omega_2) \ . \end{aligned} \tag{42}$$

Equation 42 implies that the second-order kernel will retain its shape but increase linearly in absolute size with increasing μ (provided, of course, that ϵ is small). These results are supported by our computer simulations.

NONLINEAR FEEDBACK IN SOME SENSORY BIOSYSTEMS

Retinal Cells

Extensive applications of the Wiener (white-noise) approach have been made to the study of retinal cells. In these studies, the experimental stimulus consists of white-noise modulation of light intensity about a constant level of illumination, and the re-

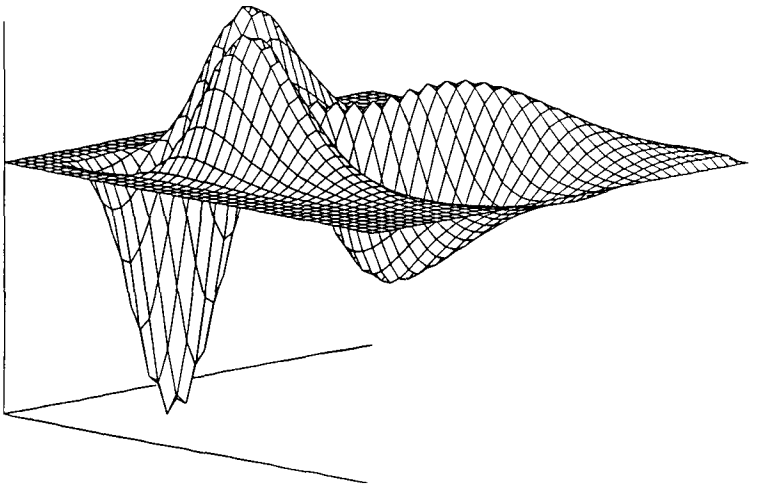

FIGURE 26. Exact second-order Wiener kernel of the system described in the caption of Fig. 25.

sponse is the intracellular or extracellular potential of a certain retinal cell. Wiener kernels (typically of first and second order) are subsequently computed from the stimulus/response data. The experiment may be repeated for different levels of constant illumination (input mean) and various white-noise input power levels. It has been observed that the waveform of the resulting kernels for some retinal cells varies with different input mean and/or power level. We propose that these changes in waveform may be explained by the presence of a nonlinear feedback mechanism, in accordance with the analysis and discussion of the previous sections. Note that these changes cannot be explained by simple cascade models that have been studied previously and reported in the literature.

The first such observation was made in the early 1970s (10) on first-order Wiener kernel estimates of horizontal cells in the catfish retina, obtained for two different levels of stimulation (low and high mean levels with proportional GWN modulation). The kernel corresponding to high level of stimulation was less damped and had shorter latency (shorter peak-response time). This observation was repeated many times later (e.g., [17]), and a gradual transition to less damped and faster (shorter latency time) waveforms was observed with increasing P and μ. These changes are qualitatively similar to the ones observed in our simulations of negative decompressive (cubic) feedback systems with overdamped linear forward subsystem. However, the changes in latency time and kernel size are much more pronounced in the experimental kernels than in our simulations of negative cubic feedback presented earlier.

To account for the experimentally observed greater reduction in kernel size, we may introduce a compressive (static) nonlinearity in cascade with the overall feedback system that leads to an additional reduction of the gain of the overall cascade system as P and/or μ increase. On the other hand, a greater reduction in the peak-response (latency) time may require the introduction of another dynamic component in cascade with the feedback system.

Led by these observations, we propose the block-structured model, shown in Fig. 27, for the light-to-horizontal cell system. This model is comprised of three

decompressive (cubic) feedback systems with different forward components (all linear and overdamped) and a compressive (static) nonlinearity in cascade, as shown in Fig. 27. The first part of this cascade model, comprised of the *PL/PN* feedback loop and the compressive nonlinearity *CN*, corresponds to the transformations taking place in the outer segment of the photoreceptor and represents the nonlinear dynamics of the phototransduction process. The second part, comprised of the *RL/RN* feedback loop, represents the nonlinear dynamic transformations taking place in the inner segment of the photoreceptors (including the receptor terminals). The third part, comprised of the *HL/HN* feedback loop, represents the nonlinear dynamic transformations taking place in the horizontal cell and its synaptic junction with the receptor. Note that the model, at this point, does not differentiate between cone/rod receptors and does not take into account spatial interactions.

When the model is simulated for GWN stimuli and parameter values judiciously chosen (as indicated in the caption of Fig. 27), the first-order Wiener kernels can be estimated using our latest Laguerre expansion technique. The results are shown in Fig. 28 for GWN input power levels $P = 0.5$, 1, 2, and 4. We observe waveform changes that resemble more closely the experimentally observed (note that hyperpolarization is plotted as a positive deflection). Since experimentally obtained horizontal-cell kernels are usually plotted in the contrast sensitivity scale (i.e., scaled by the GWN input power level), we show the same simulation results in contrast sensitivity scale in Fig. 29. The purpose of this demonstration is to show that the experimentally observed waveform changes can be reproduced fairly well by a model of this form employing nonlinear feedback. The selected model components and parameters do not necessarily correspond to physiologically accurate ones. The latter must be determined by repeated experiments (for different values of P and μ) and kernel analysis in the presented context for each particular physiological preparation.

The possibility of nonlinear feedback in the receptor-horizontal cell complex in the retina has been postulated in the past (10), and the presented simulations seem to provide additional support for this hypothesis. Greater changes in first-order kernel waveform have been observed in experiments that used steady illumination for the surround (annulus) of the receptive field of the horizontal cell (17) in addition to GWN stimulus at the center (spot). This is consistent with the hypothesis that surround stimulation makes a stronger contribution to the nonlinear feedback mechanism, possibly due to the integrative function of the horizontal cell over the surround

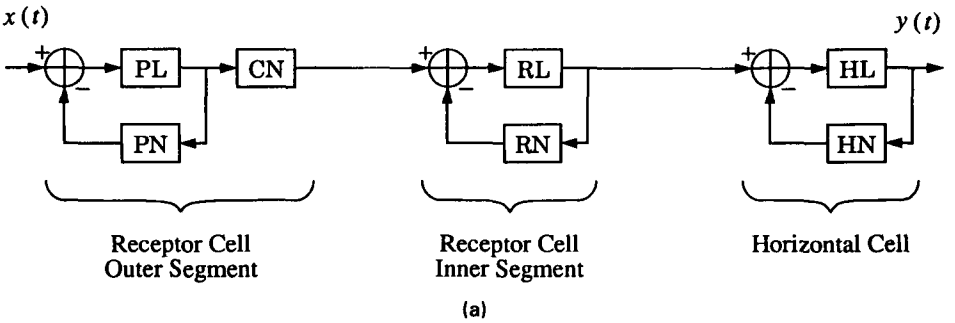

FIGURE 27. (a) Schematic of the block-structured model of light → horizontal cell system. Input $x(t)$ represents the light stimulus and output $y(t)$ the horizontal cell response. ***(Figure continued on following page.)***

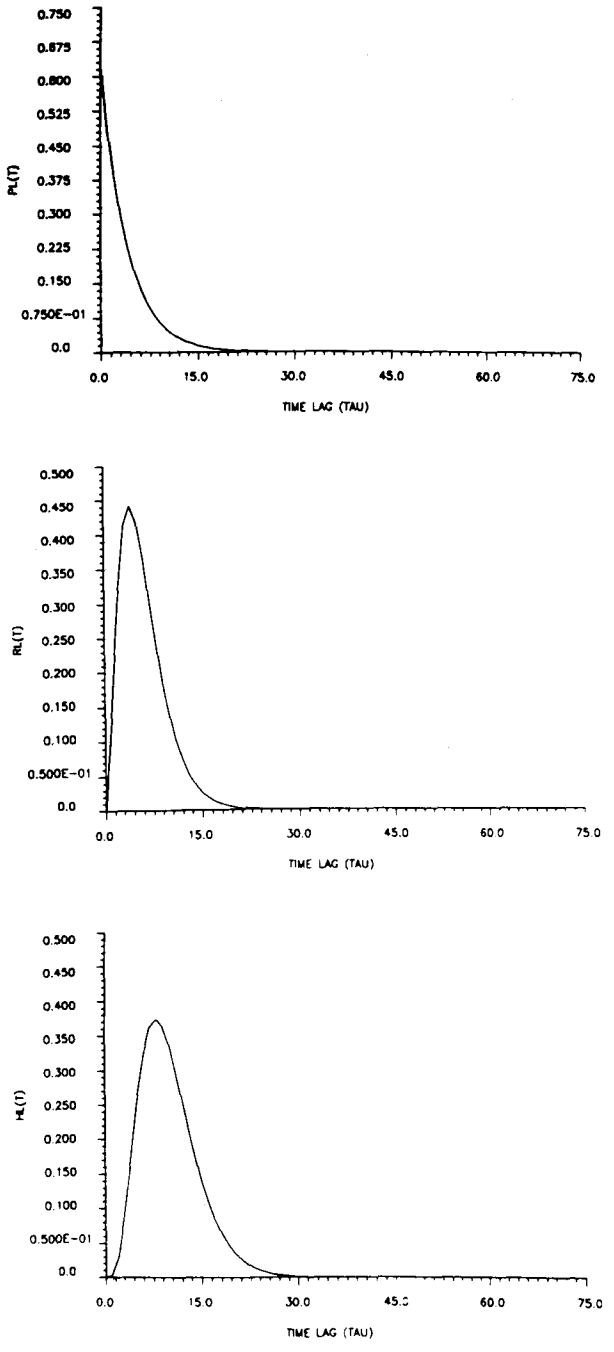

(b)

FIGURE 27 continued. (b) Impulse response functions of the linear time-invariant forward subsystems *PL*, *RL*, and *HL* used in simulations. Note that the static feedback nonlinearities *PN*, *RN*, and *HN* used in simulations are cubic of the form shown in Fig. 6 with coefficients $\epsilon = 0.05$, 0.10, and 0.01, respectively. The static nonlinarity *CN* is sigmoid of the form shown in Fig. 15 and described by Eq. 41 with $\epsilon = 2$, $\alpha = 0.2$.

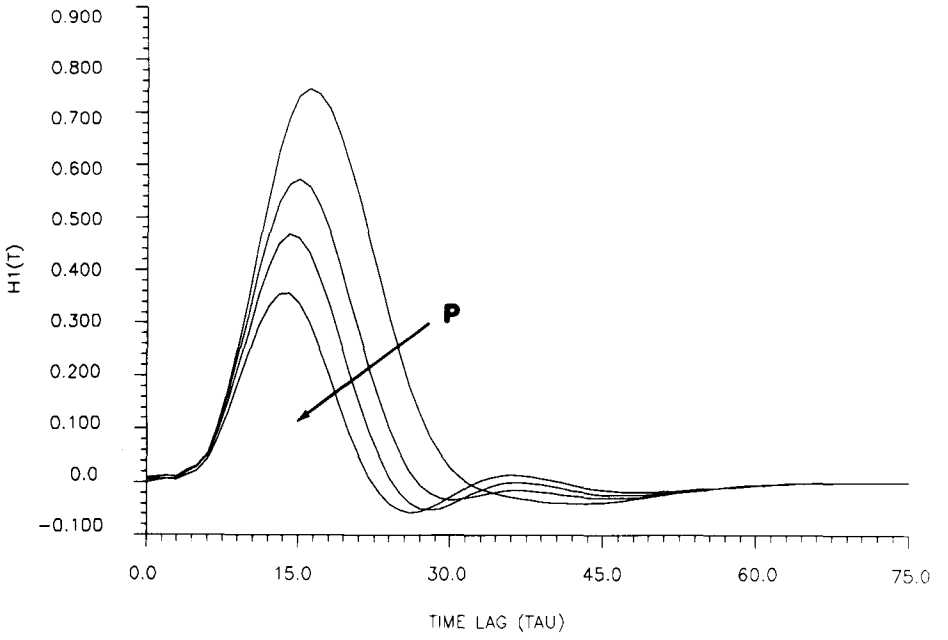

FIGURE 28. First-order Wiener kernels of horizontal cell model shown in Fig. 27(a), for $P = 0.5$, 1, 2, and 4. Observe the gradual transition in kernel waveform akin to the experimentally observed.

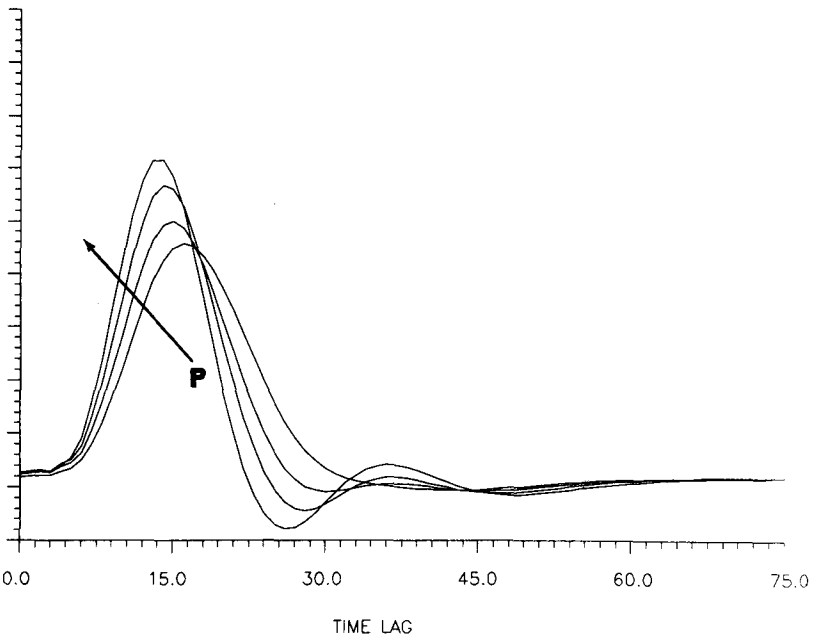

FIGURE 29. The same as in Fig. 28, with the kernels plotted in contrast sensitivity scale (i.e., each kernel multiplied by its corresponding power level).

of the receptive field, that triggers the nonlinear feedback to the centrally active receptors. The presented analysis offers the quantitative means for testing this hypothesis rigorously and for estimating the form of this nonlinear feedback on the basis of Eq. 34 using experimental kernel measurements obtained for various values of P and μ.

In a similar fashion, the experimentally observed changes in the waveform of bipolar-cell first-order kernels (for increasing GWN input power level) can be replicated by extending this model to include the bipolar cell processing level. As shown in Fig. 30, the response of the horizontal cell is subtracted from the response of the receptor (inner segment), and the resulting signal is passed through a nonlinear feedback component representing the synapses (from the receptor terminals to the horizontal processes and bipolar dendrites) as well as the transformation of the postsynaptic potential through the bipolar dendrites. The resulting first-order kernel estimates are shown in Fig. 31, and they depict the experimentally observed changes (i.e., shorter latency, increased bandwidth, and increased sensitivity with increasing P).

Beyond these mechanistic explanations, the important scientific question can be posed about the teleological reasons for the existence of decompressive feedback in retinal cells, in tandem with compressive nonlinearities. The presented simulations and the resulting models seem to suggest that this is an effective functional design that secures sensory transduction over a very broad range of stimulus intensities while, at the same time, provides adequate (practically undiminishing) dynamic range of operation about a dynamically changing operating point (attuned to changing stimulus conditions). Furthermore, the gradual transition of the system functional characteristics to an underdamped and shorter-latency response as the stimulus intensity increases provides for faster response and is more attuned to changes in sensory processing when the stimulus intensity and temporal changes are greater. This would be a suitable attribute for a sensory system that has probably evolved under the requirements of effective detection of changes in the visual field (threat detection) for survival purposes.

Auditory Fibers

An interesting example of a band-pass sensory system whose first-order Wiener kernel undergoes a transition to lower resonance frequencies as the input power level increases is found in auditory nerve fibers that have center (resonance) frequencies between 1.5 and 6 KHz. These experimental studies were conducted with pseudorandom binary stimuli that yield a set of kernels akin to Wiener kernels.

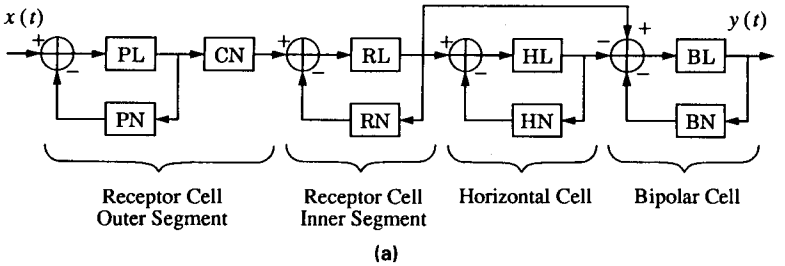

FIGURE 30. (a) Schematic of the block-structured model of light → bipolar cell system, which is an extension of the light → horizontal cell model shown in Fig. 27, as described in the text. ***(Figure continued on facing page.)***

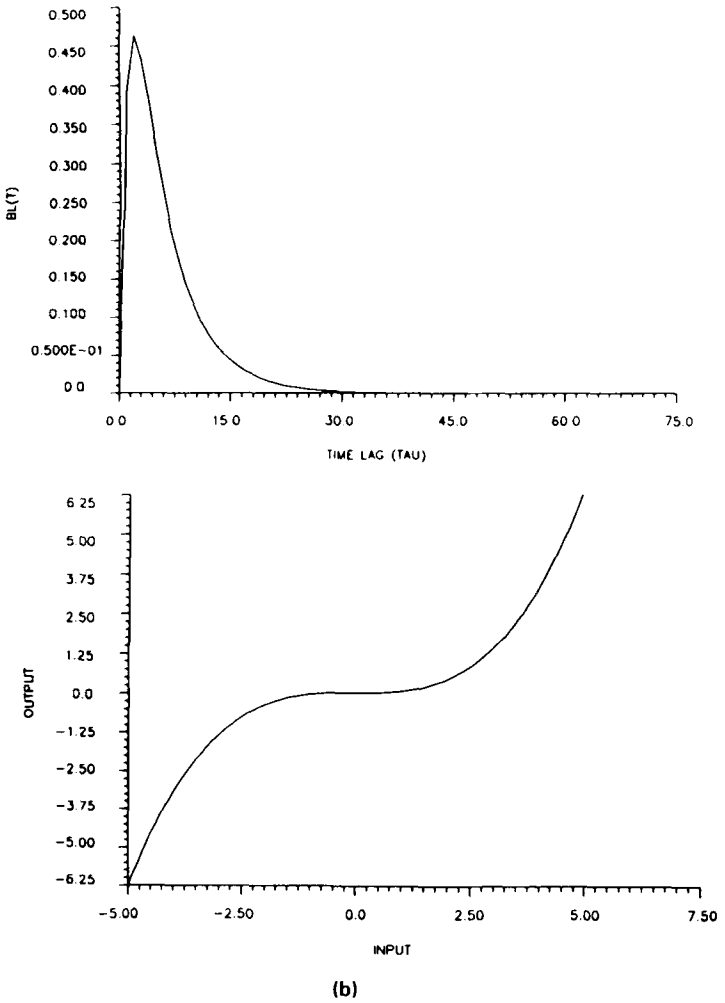

(b)

FIGURE 30 continued. (b) Impulse response function of linear time-invariant forward subsystem *BL*, and static feedback nonlinearity *BN* used in simulations.

To explore whether nonlinear feedback may constitute a plausible model in this case, we consider a band-pass linear forward subsystem with impulse response function shown in Fig. 32. In accordance with our analysis, the experimentally observed changes may be reproduced if a negative compressive (e.g., sigmoid) or positive decompressive (e.g., cubic) feedback is included in the model. Since the system remains stable for a very broad range of stimulus intensity, we consider the case of negative sigmoid feedback, like the one shown in Fig. 15 for $\epsilon = 1$ and $\alpha = 0.25$. The obtained first-order Wiener kernel estimates for GWN input power level $P = 1$, 16, 256, and 4096 are shown in Fig. 33 (with appropriate plotting offsets to allow easier visual inspection). We observe the gradual contraction of the "envelope function" and the resonance frequency of the kernel with increasing P, which were also observed experimentally (15). Since these changes are more easily seen in the frequency domain (the preferred domain in auditory studies), we also show the FFT magnitudes of these

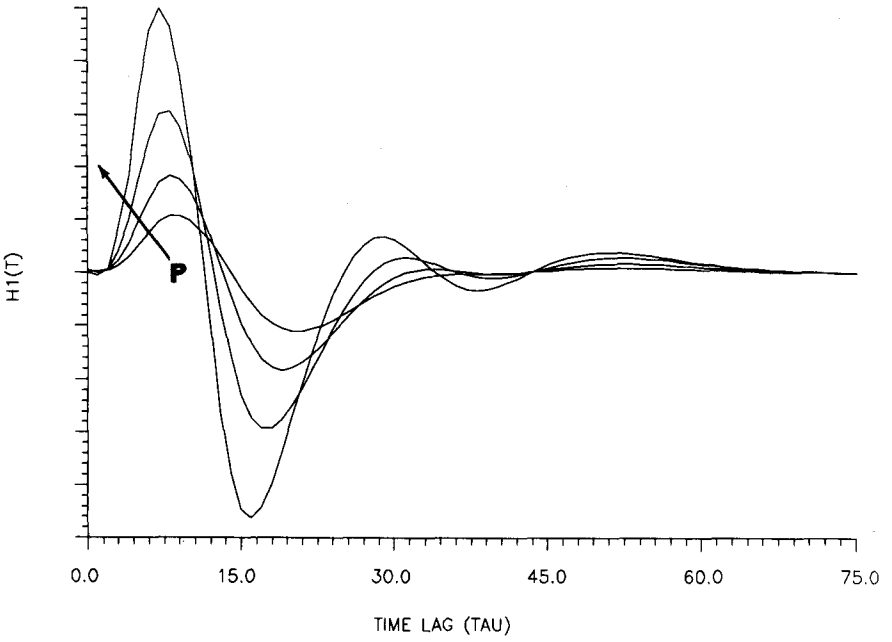

FIGURE 31. First-order Wiener kernels of bipolar cell model shown in Fig. 30(a), for $P = 0.5$, 1, 2, and 4. Observe the gradual transition in kernel waveform akin to the experimentally observed.

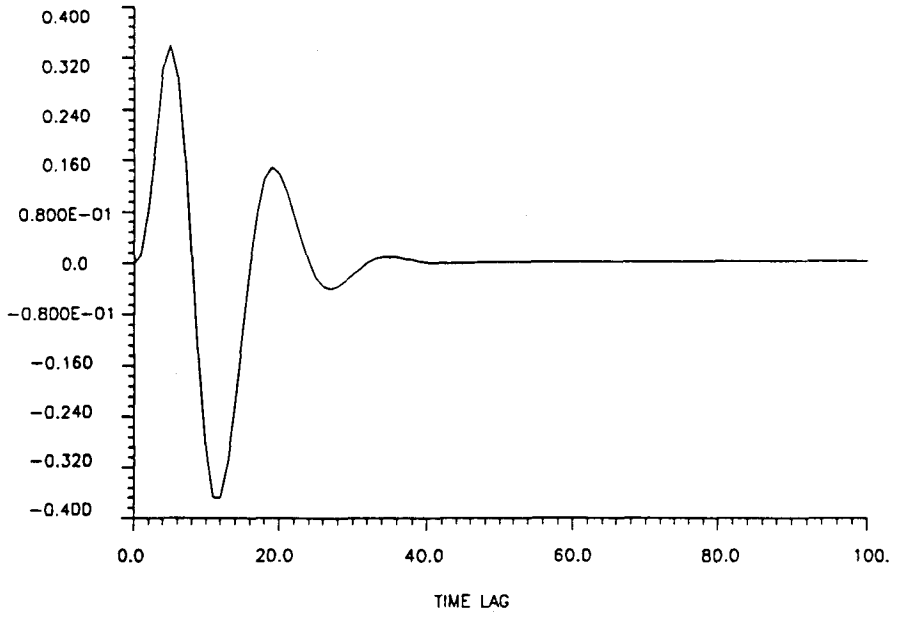

FIGURE 32. Impulse response function of band-pass linear forward used in simulation of negative sigmoid feedback system, emulating an auditory nerve fiber.

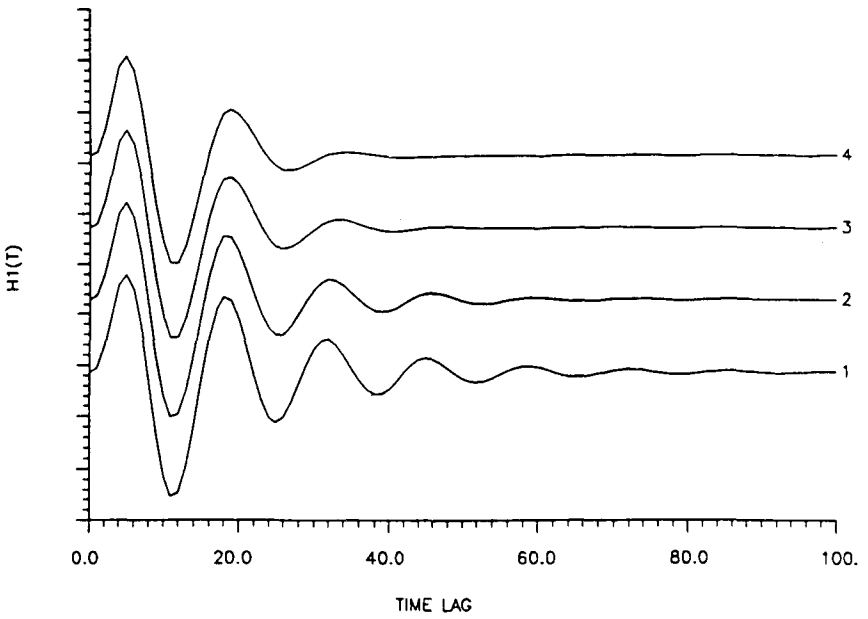

FIGURE 33. First-order Wiener kernels of negative sigmoid feedback system ($\epsilon = 1$, $\alpha = 0.25$) with the band-pass forward of Fig. 32, for $P = 1$ (trace 1), 16 (trace 2), 256 (trace 3), and 4096 (trace 4). Observe the contracting envelope and decreasing resonance frequency as P increases.

kernels in Fig. 34. These are equivalent to inverted tuning curves, and they exhibit decreasing resonance frequency and broadening of the tuning curve as P increases, similar to the experimental observations in auditory nerve fibers.

This nonlinear feedback model appears to capture the essential functional characteristics of primary auditory fibers (at least qualitatively) that have been observed experimentally. The negative compressive feedback can be thought as intensity-reduced stiffness, which has been observed in independent studies of the transduction properties of cochlear hair cells. More accurate quantitative measures of the functional components and parameters of this feedback system (e.g., the precise form of the feedback nonlinearity) can be obtained on the basis of the analysis presented earlier (see "Sigmoid Feedback Systems"), but they will require a series of properly designed white-noise experiments. Furthermore, the presence of a negative compressive feedback in the auditory fiber response characteristics may provide a plausible explanation for the onset of pathological conditions such as tinnitus, as a situation where the strength of the compressive feedback increases beyond normal values and leads to undiminishing oscillatory behavior irrespective of auditory input. This was demonstrated earlier through computer simulations of such feedback systems.

CONCLUSIONS

Wiener kernels of physiological systems have been measured experimentally in recent years, using GWN or binary/ternary stimuli of various power levels and mean

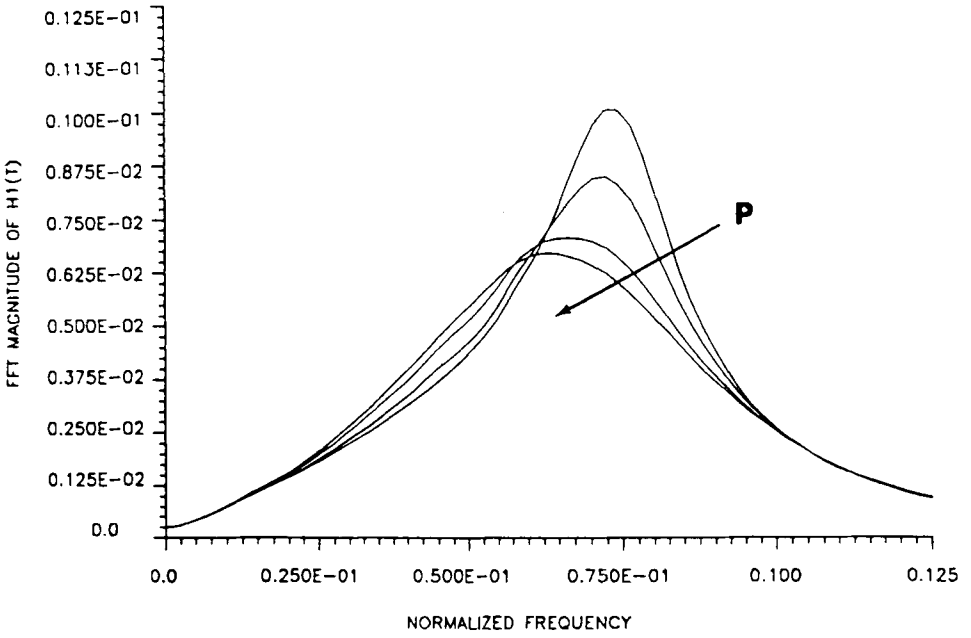

FIGURE 34. FFT magnitudes of the kernels shown in Fig. 33. We observe decreasing resonance frequency and gain as *P* increases, as well as broadening of the tuning curve in reverse relation to the envelope of the band-pass response characteristics. When these curves are plotted in contrast sensitivity scale (i.e., each multiplied by its corresponding *P* value), then the resonance-frequency gain will appear, increasing with increasing *P*.

levels. They have often exhibited changes in waveform and size for different mean and power levels of the stimulus. Models that employ nonlinear feedback can account for such changes in kernel waveform.

Nonlinear feedback has been long thought to exist in many important physiological systems, but its systematic and rigorous study has been hindered by the complexity (and often inadequacy) of the analytical methods used. The study of Volterra-Wiener expansions of nonlinear differential equations has led to some analytical results that begin to shed light on the important question of Wiener analysis of nonlinear feedback systems. This article presents some results, obtained for a class of nonlinear feedback systems, that relate Wiener kernel measurements with the effects of nonlinear feedback under various experimental conditions. It addresses the question, What kind of changes in kernel waveform (as a result of varying stimulus conditions) can a nonlinear feedback model explain? Explicit mathematical expressions are presented that relate Wiener kernel measurements to the characteristics of the feedback system and the stimulus parameters. The theoretical results were tested with simulations, and their validity was demonstrated in a variety of cases (cubic and sigmoid feedback with overdamped, underdamped, or band-pass linear forward subsystem). These test cases were chosen as to suggest possible interpretation of experimental results that have

been published in recent years for two types of sensory systems: retinal horizontal and bipolar cells, and auditory nerve fibers. It was shown that relatively simple nonlinear feedback models can be constructed that reproduce the qualitative changes in kernel waveforms observed experimentally in these sensory systems. Precise quantitative determination of feedback models requires analysis (in the presented context) of a series of properly designed experimental data.

Specifically, it was shown that negative decompressive feedback (e.g., cubic) or positive compressive feedback (e.g., sigmoid) result in gradually decreasing damping (increasing bandwidth) of the first-order Wiener kernel as the GWN input power level and/or mean level increase. Conversely, positive decompressive or negative compressive feedback result in the reverse pattern of changes. The extent of these effects depends, of course, on the exact type of feedback nonlinearity and/or linear forward subsystem. There are also companion effects on the kernel size and system sensitivity (i.e., zero-frequency or resonance-frequency gain). It was demonstrated through analysis and computer simulations that the experimental observations of first-order Wiener kernel measurements for retinal horizontal and bipolar cells can be qualitatively explained with the use of negative decompressive (cubic) feedback and low-pass linear forward subsystems (viz., the gradual transition from an overdamped to an underdamped mode as the GWN stimulus power and/or mean level increase). In the case of auditory nerve fibers, it was shown that the use of negative compressive (sigmoid) feedback and a band-pass linear forward subsystem can reproduce qualitatively the effects observed experimentally on their tuning curves for increasing stimulus intensity (viz., a gradual downward shift of the center frequency and broadening of the tuning curve with increasing stimulus power level).

The effect of quadratic feedback on the second-order Wiener kernels was also discussed and demonstrated through computer simulations. Likewise, the emergence of second-order Wiener kernels when GWN inputs with nonzero mean are used in probing cubic or sigmoid feedback systems was discussed, and agreement with our theoretical derivations was demonstrated through simulations.

It is hoped that this work will inseminate an interest among systems neurophysiologists to explore the possibility of nonlinear feedback models to explain changes in Wiener kernel waveforms when the experimental stimulus conditions (i.e., power and mean level) vary. These changes in kernel waveform cannot be explained by simple cascade models of linear and static nonlinear components, which are currently popular in efforts to construct equivalent block-structured models from Wiener kernel measurements. The nonlinear feedback models may offer compact representations of the stimulus-response nonlinear dynamic relationship in these cases and may lead to physiologically meaningful interpretations of the system function. For instance, in the case of the auditory nerve fibers, the suggested model of negative sigmoid feedback may signify the gradually decreasing stiffness of hair cells as the sound stimulus intensity increases and may offer a plausible explanation for pathological states of the auditory system, such as tinnitus. Likewise, in the case of retinal cells, negative decompressive feedback in tandem with compressive nonlinearities may explain the ability of the "front end" of the visual system to accommodate a very broad range of visual stimulus intensities while preserving adequate dynamic range for effective information processing, as well as the ability to remain attuned to changes in stimulus conditions.

REFERENCES

1. Barrett, J.F. The use of functionals in the analysis of nonlinear physical systems. J. Electron. Control 15:567–615; 1963.
2. Barrett, J.F. The use of Volterra series to find region of stability of a nonlinear differential equation. Int. J. Control 1:209–216; 1965.
3. Bedrosian, E.; Rice, S.O. The output properties of Volterra systems (nonlinear systems with memory) driven by harmonic and Gaussian inputs. Proc. IEEE 59:1688–1707; 1971.
4. Korenberg, M.J. Identification of nonlinear differential systems. Proc. Joint Autom. Cont. Conf. 597–603; 1973.
5. Korenberg, M.J. Identification of biological cascades of linear and static nonlinear systems. Proc. Midwest Symp. Circuit Theory 18(2):1–9; 1973.
6. Korenberg, M.J. Functional expansions, parallel cascades and nonlinear difference equations. In: Marmarelis, V.Z., ed. Advanced methods of physiological system modeling: Vol. I. Los Angeles: Biomedical Simulations Resource, University of Southern California; 1987: pp. 221–240.
7. Korenberg, M.J. Identifying nonlinear difference equation and functional expansion representations: The fast orthogonal algorithm. Ann. Biomed. Eng. 16:123–142; 1988.
8. Lee, Y.W.; Schetzen, M. Measurement of the Wiener kernels of a nonlinear system by cross-correlation. Int. J. Control 2:237–254; 1965.
9. Marmarelis, P.Z.; Marmarelis, V.Z. Analysis of physiological systems: The white-noise approach. New York: Plenum; 1978. Russian translation, Moscow: Mir Press; 1982.
10. Marmarelis, P.Z.; Naka, K.-I. Nonlinear analysis and synthesis of receptive-field responses in the catfish retina. J. Neurophysiol. 36:634–648; 1973.
11. Marmarelis, V.Z., ed. Advanced methods of physiological system modeling: Vol. I. Los Angeles: Biomedical Simulations Resource, University of Southern California; 1987.
12. Marmarelis, V.Z., ed. Special issue on nonlinear modeling of physiological systems. Ann. Biomed. Eng. 16(1); 1988.
13. Marmarelis, V.Z., ed. Advanced methods of physiological system modeling: Vol. II. New York: Plenum; 1989.
14. Marmarelis, V.Z. Identification and modelling of a class of nonlinear systems. Math. Comput. Mod. 12:991–995; 1989.
15. Moller, A.R. Frequency selectivity of phase-locking of complex sounds in the auditory nerve of the rat. Hear. Res. 11:267–284; 1983.
16. Rugh, W.M. Nonlinear system theory: The Volterra/Wiener approach. Baltimore: Johns Hopkins Univ. Press; 1981.
17. Sakai, H.M.; Naka, K.-I. Signal transmission in the catfish retinal (V). J. Neurophysiol. 58:1329–1350; 1987.
18. Schetzen, M. The Volterra and Wiener theories of nonlinear systems. New York: Wiley; 1980.
19. Shi, J.H.; Sun, H.H. Nonlinear system identification for cascaded block model: An application to electrode polarization impedance. IEEE Trans. Biomed. Eng. 37:574–587; 1990.
20. Volterra, V. Theory of functionals and of integral and integro-differential equations. New York: Dover; 1930.
21. Wiener, N. Nonlinear problems in random theory. New York: Wiley; 1958.